國立交通大學

電控工程研究所

碩士論文

用於復健任務導向訓練之穿戴式手指研發

Development of Wearable Robotic Fingers for Rehabilitation Applications

研究生：蔡依穎

指導教授：宋開泰 教授

中華民國一百零二年七月

用於復健任務導向訓練之穿戴式手指研發

Development of Wearable Robotic Fingers for Rehabilitation Applications

研 究 生：蔡依穎　　Student：Chai Yea Yen

指導教授：宋開泰 教授　　Advisor：Dr. Kai-Tai Song

國 立 交 通 大 學
電 控 工 程 研 究 所
碩 士 論 文

A Thesis
Submitted to Institute of Electrical Control Engineering
College of Electrical and Computer Engineering
National Chiao Tung University
in Partial Fulfillment of the Requirements
for the Degree of Master
in
Electrical Control Engineering
July 2012

Hsinchu, Taiwan, Republic of China

中 華 民 國 一 百 零 二 年 七 月

用於復健任務導向訓練之穿戴式手指研發

學生：蔡依穎　　指導教授:宋開泰　博士

國立交通大學電控工程研究所

摘要

隨著老年人口逐年增加，復健治療的品質受到更廣泛的重視，許多學者專家開發了各種用途的復健機構來輔助中風病患進行復健。本論文研究基於任務導向治療之抓取訓練，設計了一個具有三個自由度的穿戴式手指機構，同時考量到使用者意圖及在任務中抓取物體的舒適性及安全性，我們提出了一套控制策略來完成輔助抓取的任務。所發展之控制策略分為兩部份：使用者順應性控制與抓取順應性控制。在使用者順應性控制中，當使用者產生抓物意圖施予力道時，能夠利用質量—彈簧—阻尼物理模型來順應使用者的力道讓使用者感到舒服並且容易隨著所施予的力道來控制手指機構；而在抓取順應控制中，基於同樣的物理模型來控制，當手指外骨骼在移動的過程中，如果與物體接觸時能夠即時的感知並控制抓取的力道以完成穩定抓取，並避免使用者在抓取訓練的過程中受到傷害。透過本設計的實現，可以確保使用者穿戴此機構在抓取訓練的過程中的舒適性及安全性考量。經過實驗證實，我們設計的穿戴式手指機構能夠讓使用者感到舒適以及能夠輔助使用者完成抓取的任務。

Development of Wearable Robotic Fingers for Rehabilitation Applications

Student：Chai Yea Yen Advisor：Kai-Tai Song

Institute of Electrical Control Engineering
National Chiao Tung University

Abstract

With the increase of stroke patients, the quality of stroke rehabilitation has drawn much attention in recent years. Researchers have been developed various kinds of exoskeleton devices for specific rehabilitation functions. In this thesis, we have developed a 3 Degrees of Freedom (3DOF) wearable robotic fingers for task-oriented training of rehabilitation grasping tasks. We propose a control strategy for the task training considering user comfort based-on his/her intention and the safety in task training procedure. The control strategy is divided into two parts: user compliance control and grasping compliance control. In user compliance control, we employed a mass-spring-damper model for grasping operation when the user exerted an intention force, this strategy can allow the user to feel comfortable guidance of the movement. In grasping compliance control, a similar physical model is used when the finger exoskeleton comes into contact with the object, that the system will percept the situation immediately and assists an appropriate grasping force for stable grasping. Experimental verification shows that the developed wearable rehabilitation robotic fingers can provide a comfortable fit for the users and is capable to assist the users to achieve the grasping task training.

Acknowledgments

I am very grateful to the people who have been sharing this whole experience with me. I would like to thank my advisor Professor Kai-Tai Song for his advice, guidance and help and I appreciate all that I have learned from him. I would like to thank my oral defense committee members Jwu-Sheng Hu, Chwan-Hsen Chen and Hsien-I Lin for taking time off their busy schedules to review and provide assistance on my work. I also thank to all members of the Intelligent Systems and Control integration Lab who were always very kindly and helpfully whenever I needed. Finally, I thank my parents, brother, sisters and my boyfriend for their constant support and encouragement.

Content

List of figures

List of tables

I. Introduction

1.1 Motivation

Stroke is the second leading cause of death and one of the leading causes of adult disability worldwide. In Taiwan, the average incidence of stroke is about 3 per 1,000 people and affects approximately 30,000 people per year, most aged 35 and above [1]. Stroke incidence and mortality significantly increase with aging. According to the America National Stroke Association [2], the current statistics for stroke survival rates are shown in the Fig. 1.1. In Fig. 1.1, we see that most of the stroke survivors are unable to perform activities of daily life (ADL) and causes increasing demand for the practical application of assistance and rehabilitation technologies. Approximately 38% of stroke survivors reported that impaired hand function is the most disabling motor impairment they face [3]. Further, the post-stroke rehabilitation plays an important role in stroke recovery because highly repetitive exercises can help to restore the motor function [4].

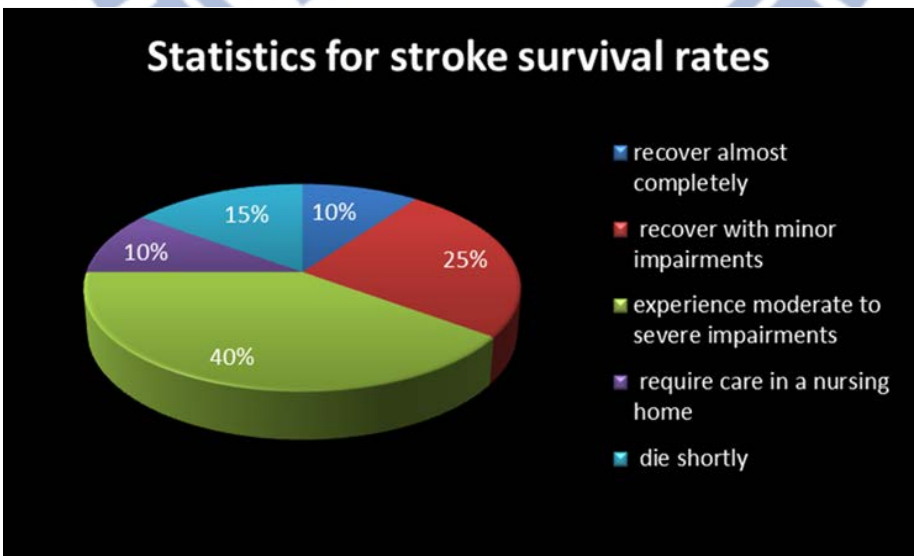

Fig. 1.1: U.S. Statistics for stroke survival rates in [2].

However, conventional therapy remains suboptimal due to human resources and the quantitative evaluation of the patient's performance is difficult with conventional therapy. In order to improve the quality of life, we want to develop a wearable rehabilitation robotic hand to assist the stroke survivors to achieve the task-oriented training specifically for grasping object. This study focuses on the mechanical design for hand exoskeleton and proposes a control strategy to assist the stroke patients to accomplish task-oriented training in grasping different weights of objects.

1.2 Background

1.2.1 Anatomy of hand

The hand is primary an effector organ for our most complex motor behavior, the elements of the hand skeleton can be divided into three parts: the eight carpals, the five metacarpals, and the fourteen of hand phalanges with a total of 27 bones [5]. There are eight short bones of the carpus organized into a proximal row (scaphoid, lunate, triquetrum and pisiform), which articulates with the skeleton of the forearm, and a distal row (trapezium, trapezoid, capitate and hook of hamate), which articulates with the bases of the metacarpal bones. Together with the fourteen phalanx bones of the fingers these, metacarpal bones form a poly-articulated chain. In addition, the hand has five metacarpals, often referred to collectively as the "metacarpus". Each of the digits contains a set of phalanges. In Fig. 1.2, from right side to left side are the thumb, index, middle, ring, and small fingers respectively. The articulations between the proximal end of the metacarpals and the distal row of carpals bones form the

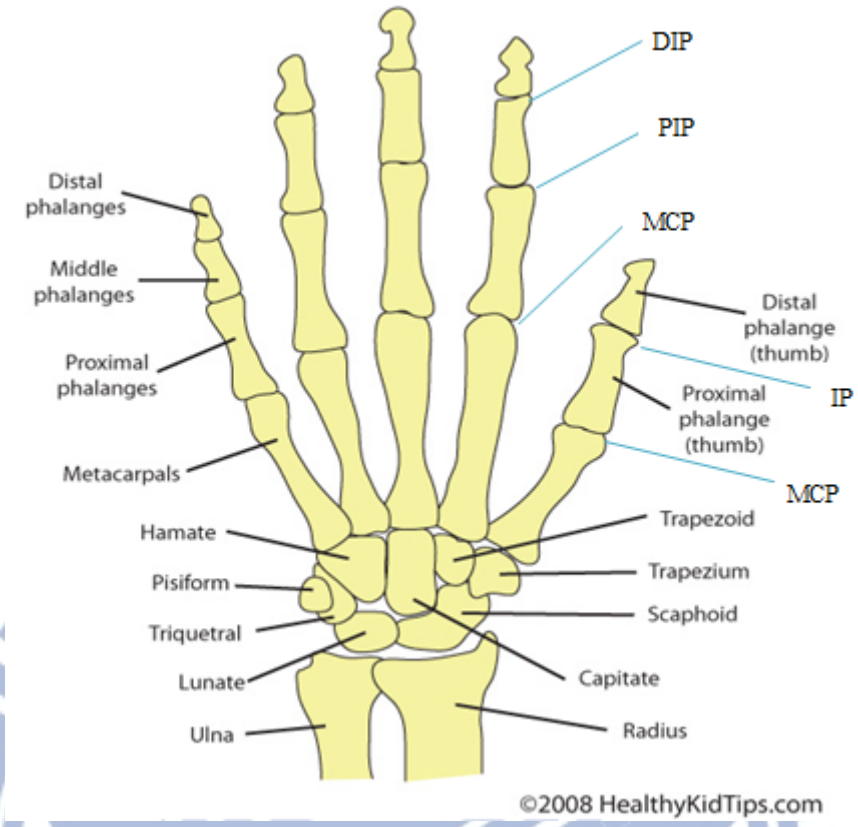

Fig. 1.2: Human hand skeleton in [7].

carpometacarpal (CMC) joints. The articulations between the metacarpals and the proximal phalanges form the metacarpophalangeal (MCP) joints. Each finger has two interphalangeal joints: a proximal interphalangeal (PIP) and a distal interphalangeal (DIP). The thumb has only two phalanges and an interphalangeal (IP) joint [6].

The human hand skeleton consists of 27 degrees of freedom (DOF) [8], each of the four fingers has 4 DOF. Every distal interphalangeal (DIP) joint and proximal interphalangeal (PIP) joint have 1 DOF. The metacarpophalangeal (MCP) joint has 2 DOF for flexion and abduction functioning. The thumb has a different structure from the other four fingers and has 5 DOF, one for the interphalangeal (IP) joint, two for MCP joint and trapeziometacarpal (TM) joint both for flexion and abduction. Finally, each of the palm translational and rotational motion consist of 3 DOF. The range motion of the hand is the amount of movement when moving a joint from a starting

position to the end position within the natural range. It varies depending on the particular joint and the health of the articulation. The average range of hand motion is shown in Table 1.1 [9]. Besides, the PIP and DIP joints are not independent and the relations can be described as $\theta_{DIP} = \frac{2}{3}\theta_{PIP}$ [10].

The mechanism functioning and a hand exoskeleton are closely related when it is worn. The basic knowledge of hand anatomy and biomechanics are important development for assistive hand exoskeleton. In an attempt to ensure a safe and effective training procedure, consideration of the degree of freedom (DOF) and range of motion (ROM) of each joints are necessary for the mechanical design. These knowledge are very helpful to achieve proper functions for rehabilitation and assistance.

Table 1.1: Joints, associated motions, planes of motion in anatomical position, and average range of motion in [9].

Joint	Motion	Plane of Motion	Avg. ROM (degrees)
Thumb (MP)	Flexion	Frontal	15 (CMC & MCP)
	Extension	Frontal	20 (CMC & MCP)
	Abduction	Sagittal	70 (CMC & MCP)
Thumb (IP)	Flexion	Frontal	80
Finger (MCP)	Flexion	Sagittal	90
	Extension	Sagittal	30
Finger (PIP)	Flexion	Sagittal	100
Finger (DIP)	Flexion	Frontal	85-90

1.2.2 Task Oriented Training

The persons who are affected by stroke illness would encounter some problems like muscle and movement problems (hemiparesis/hemiplegia), communication problems (aphasia), sensory disturbances, memory thinking and emotional disturbances problems [11]. Most stroke patients are unable to perform normally for their daily tasks. Therefore, stroke rehabilitation played an important role for helping them to regain their skills and to live more independently.

In neuro-rehabilitation, task-oriented training has emerged as the dominant approach to motor restoration for stroke-induced motor impairments. Task-oriented training has been proven to have a better functional outcome compared with traditional therapies [12] and effective for the improvement of skilled arm–hand performance after stroke [13]. However, the task-oriented training is still lack of conclusively defined in the literature. Task-oriented training is based on more recent integrated models of motor control, motor learning and behavioral neuroscience, where active participation and skill acquisition are critical components of recovery [14]. This training involves practicing real-life tasks such as drinking water and grasping an object. In functional training task, the therapist will set the goals in consultation with the individual and based on evaluation of the patient's capabilities. In addition, the patients are required to think of problem solving strategies and produce their best efforts to achieve the task. Task-oriented training differs from repetitive training because the repetitive training is focused on a bottom-up approach and losing the intrinsic motivation to achieve a goal/task of acquiring a skill. On the other hand, task-oriented training will enhance intrinsic motivation of the patient for motor learning [15].

Carolee et al. [14] proposed a crucial and an effective task-oriented training

program, which is described as follows:

(a) Challenging enough to acquire new learning and engagement with intention to solve the motor problem.

(b) Progressive and optimally adapted such as over practice, the task-demand is optimally adapted to the patient's capability and the environmental context.

(c) Interesting enough to invoke active participation to engage a "particular type of repetition" that Bernstein referred to as "problem solving".

1.2.3 Compliance Control

Today, robots are widely used in factories to perform tasks that require high precision, such as assembly, packing, manufacturing and welding. However, most robots cannot perform contact tasks satisfactorily such as window cleaning, driving a screw, and assembling toys under position control. Therefore, force control must be considered instead of position control in order to avoid the dangerous situations between the robot and environment.

The compliance describes movement characteristics of contact reaction force or torque when the robots collide with the environment. The so-called compliance control, that is, when the robots contact with the environmental surfaces, the robots generate appropriate ability to adapt the environmental situation according to the contact force and the movement, both position and force control are essential. The compliance motion control can be divided into two categories: passive compliance and active compliance.

1.2.3.1 Passive Compliance

Passive compliance mainly utilizes the robot's hardware structure that deforms in response to forces caused by slight misalignment. Passive compliance differs from active compliance because it does not apply the force information as a feedback to modulate the control algorithm.

The safe joint mechanism (SJM) [16-18] in Fig. 1.3, is a passive mechanism element which enable to guarantee the positioning accuracy and collision safety. The SJM consist of an inclined link, a slider with rollers and linear springs. The SJM provides a respond to external forces immediately and absorb the collision force by using the springs. The advantage of passive mechanism is rapid response, low cost and simple structure. On the contrary, there is lack of versatility, which can only be used in specific robot only.

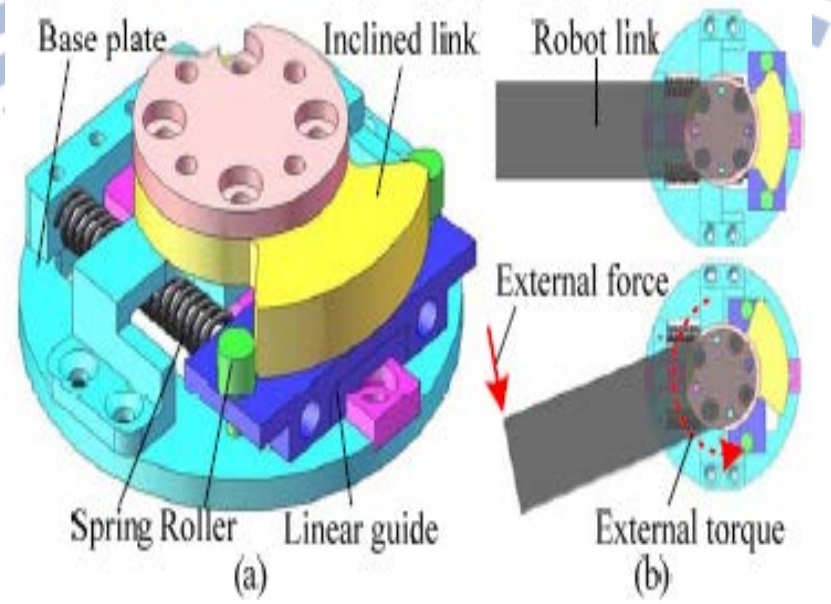

Fig. 1.3: Prototype model of SJM-III (a) 3-D CAD model (b) Operation of SJM-III in [18].

1.2.3.2 Active Compliance

Active compliance utilizes the software as a mediate to modulate the control algorithm and the hardware possessing compliance function. This method is more robust compared to passive compliance. Active compliance provides good performance from force feedback of measurements but deficient in position and speed control directly. In fact, this would cause the position and speed responses underperform. In recent years, many researchers have been using experimental studies for compliance control in order to control both position and force. The major control approaches can be divided into two parts: impedance control and hybrid position/force control.

- Impedance control:

Impedance control had been proposed by Hogan [19], he generalizes the approach of damping control and stiffness control. This approach mainly allows the robot's end-effector to act as a mass-damper-spring mechanism with the desired preset parameters, such as mass coefficient, damper coefficient and spring coefficient. Therefore, the compliance motion can be achieved when the robot's end-effector interacts with the environment by modulate the impedance parameters.

Kazerooni [20] et al. discussed the impedance control in frequency domain and designed a robust controller which is insensitive to the uncertainty in robot dynamics. Anderson and Spong [21] proposed a hybrid impedance control for the purpose to control contact forces of a robot. Liu and Goldenberg [22] utilized the computed torque technique and PI control law to reduce the influence of model uncertainties. In [23], a new position-based impedance control law that combined force feedback and position control, the trajectory tracking based on force feedback that gave the system

the desired mechanical behavior. Work in [24], the integral sliding mode control was employed to solve the problem of nonlinearities and uncertainties in the robot fingers.

- Hybrid position/force control:

Hybrid position/force control is an approach that combines conventional position control and force control. These position controls are executed in the directions where there are no constraints, otherwise the system switch to force control when the robot is in the direction where there is constraint. In 1976, Paul and Shimano [25] control the motion of robot by separating the position control loop and force control loop. Craig [26] and Mason [27] give good summaries for the hybrid control design. In [28], the authors design a force/position controller by using PID control and the work space of robot end-effector are decided through the matrices.

The computation of this method is complicated because it needs to calculate the dynamics model of the robot and the control system should change consequently for each new task.

1.3 Previous Related Works

The work to be introduced in this thesis mainly focuses on the current rehabilitation/assistance technology. In recent years, many upper limb rehabilitation devices have been developed to provide rehabilitation therapy for stroke patients. Although there are several researches proposed the rehabilitation of upper limb that included shoulder, elbow and wrist [29]-[30], robotics for hand rehabilitation is much less developed and it cannot satisfied the demand of stroke patients pursuing their quality of life. The following paragraphs will present previous analysis that reviews the development of the hand rehabilitation.

In [31], the authors designed an exoskeleton assistive hand and controlled the

movement by bioelectric potential measured from the lumbricals. The exoskeleton assistive hand in Fig. 1.4 has eleven active joints: three active joints for an index finger, two active joints for a thumb, three active joints for wrist and three active joints for combination of a middle finger, a ring finger and a little finger. The authors claimed that the exoskeleton could synchronize wearer's hand activities without force sensor by the control algorithm "bioelectric potential-based switching control". The bioelectric potential-based switching control as shown in Fig. 1.5 is divided into two parts: finger-following and grasping force control. When the measurement of grasping force is below threshold, the system controls the motors for keeping the wires slightly relaxed to allow the user to move the fingers freely. Otherwise, the system switchs to grasping force control to provide the force assistant. The integral value of bioelectric potential "IBEP" is calculated by

$$\mathrm{IBEP(t)} = \int_{t-T}^{t} bep(i)di \tag{1.1}$$

where t is time, T is the accumulation period and bep(i) is the electric potential measured at time i.

Fig. 1.4: Five fingered in assistive hand on forearm in [31].

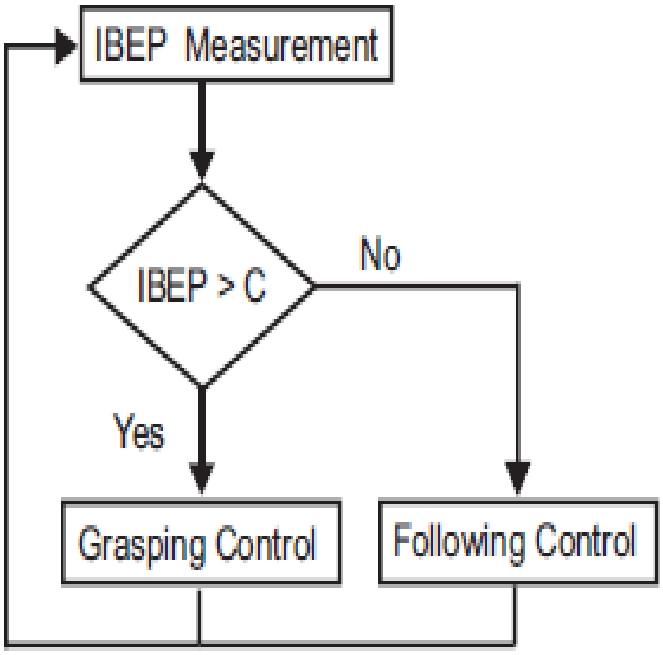

Fig. 1.5: Bioelectric potential-based switching control in [31].

In [32], the authors proposed a novel wearable device actuated by pneumatic artificial muscles to assist the stroke patients for task-oriented physical therapy performance. The mechanism of wearable rehabilitation robotic hand, as shown in Fig. 1.6, which provides a two degrees of freedom (DOFs) and consists of two pneumatic artificial muscles (PAM) attached on the top of the forearm. One of the PMAs was directly connected to the lever of the thumb and another PMA was connected with a cable passing through the travel transform pulley connected to the front lever. The Rehabilitation robotic hand control system as shown in Fig. 1.7.

The advantages of pneumatic actuator are low cost; ease at reversion movements, lightweight, safety and easy to control. However, in Fig. 1.6, we can see that the actuator is too big to attach on the robot hand, the space of robot hand is not enough to attach too many actuators.

Fig. 1.6: PAM wearable rehabilitation robotic hand in [32].

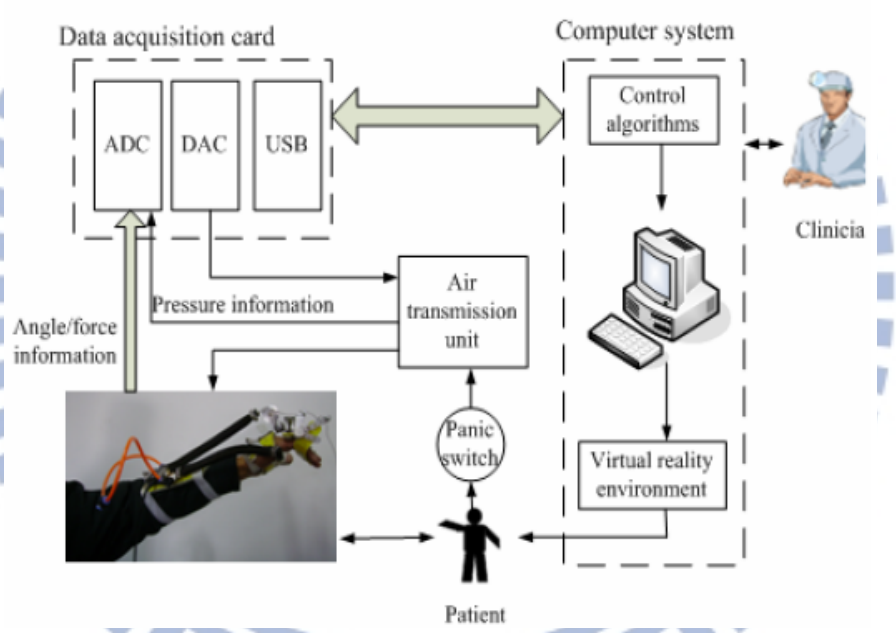

Fig. 1.7: The control system of the rehabilitation robotic hand in [32].

Yamaura et al. [33] proposed a hand rehabilitation system which provides a long-term passive rehabilitation for patients suffering from paralysis or contracture. The authors developed the wire-driven link mechanism based on the arm structure and they substitute the motor joint with a free joint. Three pulleys were attached to the free joints and the pulleys are connected by means of two wires, as shown in Fig. 1.8;

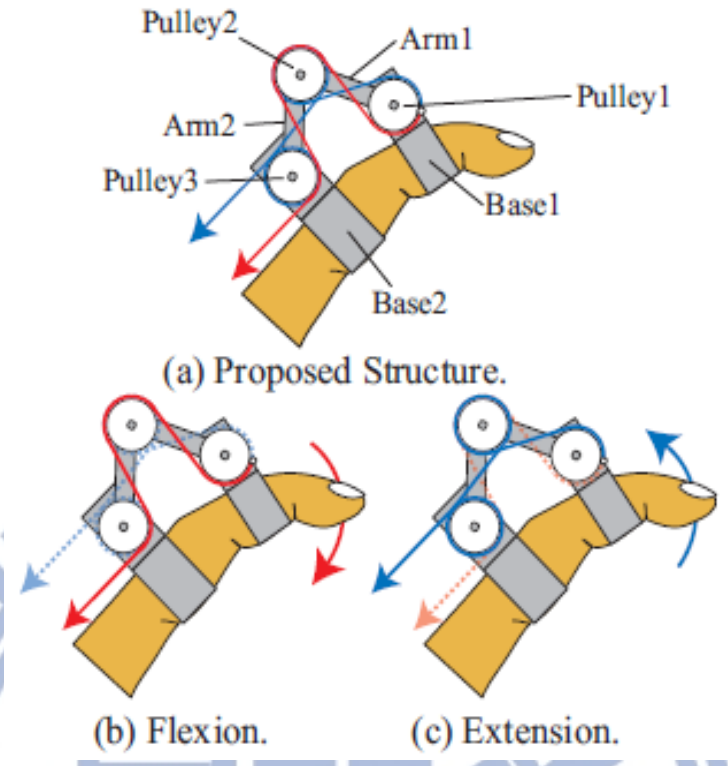

Fig. 1.8: The mechanism design in [33].

one end of each wire is attached to Base1, and the other end is attached to a motor. The red line represents a flexion wire and the blue line represents an extension wire. The hand rehabilitation system in Fig. 1.9 consists of two components: a hand rehabilitation machine, which moves human finger joints using a motor, and a data glove, which enables to control the movement of the finger joints attached to the rehabilitation machine, they use a data glove to measure the joint angles of the DIP and PIP on the index finger from the healthy hand and thus controls the motion of the paralyzed finger with a machine. This system has a motion playback function so the user can record finger movements for a maximum 10 seconds and playback the finger movements cyclically. This hand rehabilitation system can only be used by hemiplegic patients and not available for paraplegic patients who cannot achieve the self-motion control.

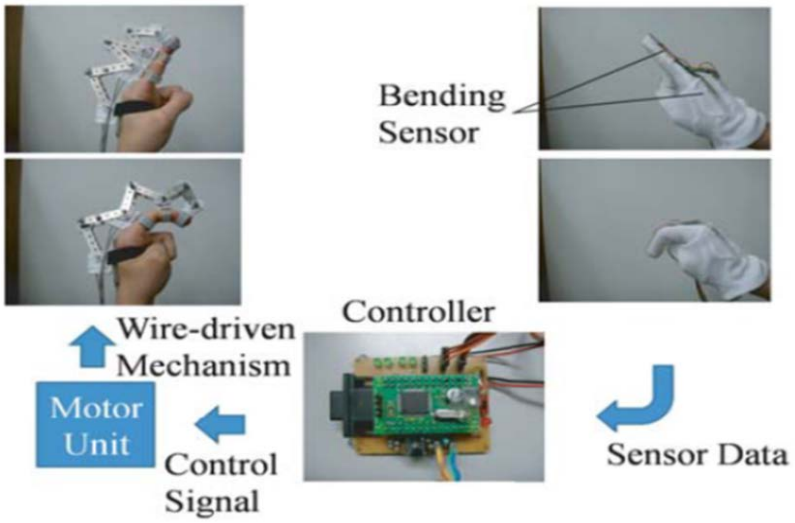

Fig. 1.9: The control system of rehabilitation hand in [33].

In [34], the authors developed a novel hand rehabilitation robot named HIT-glove driven by DC motors via Bowden cable transmission to provide patient-cooperative therapy for post-stroke patients with hand impairment. The actuated hand exoskeleton shown in Fig. 1.10, which provides 2 degrees of freedom (DOFs) for each finger, can be applied to hands in different sizes and capable to bilaterally actuate every joint of the fingers. The system architecture of the HIT-glove as shown in Fig. 1.11, it consists of an actuated hand exoskeleton, an interactive

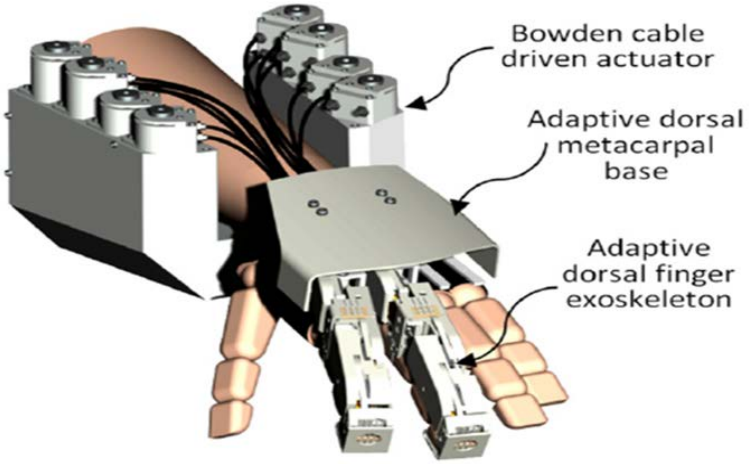

Fig. 1.10: The actuation design of hand exoskeleton in [34].

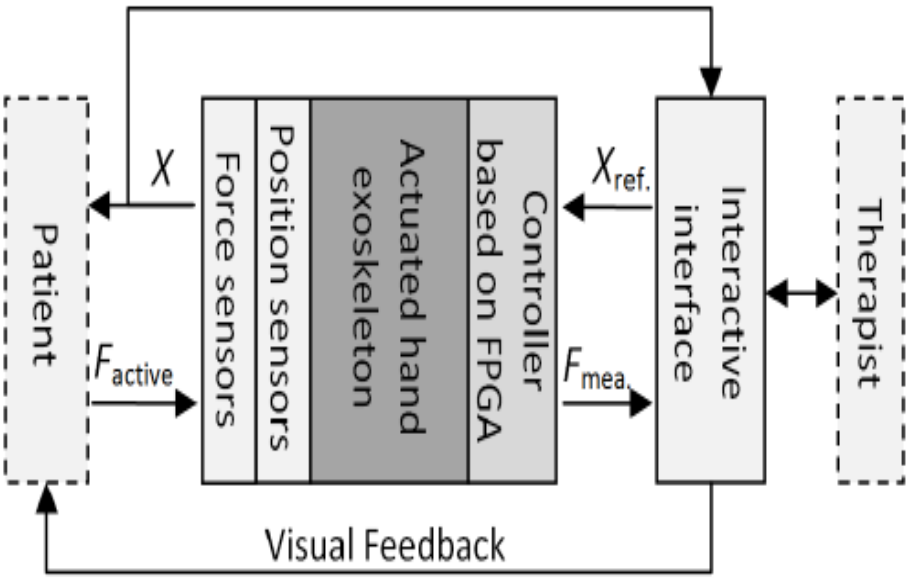

Fig. 1.11: The system architecture of the HIT-glove in [34].

interface, an electric controller and the sensing system. In the therapy training, the patients should try their best to make an active effort level. The current position will be measured by force sensors and position sensors respectively. At the same time, the interactive interfaces will give out a reference value to assist the patient according to the virtual situation in the effort level and current position training programs respectively.

In [35], the authors developed an exoskeleton hand robotic training device for stroke patients and training for impaired hand by using an exoskeleton robotic hand which is actively driven by electromyography (EMG) signals from the hemiplegic side and assists in hand opening or hand closing functional tasks. The exoskeleton hand robotic training device in Fig. 1.12, which consists of five fingers and each finger assembly provides 2 degrees of freedom (DOFs). For each finger at the MCP and PIP together by the mechanical linkage system which actuated by a single linear actuator.

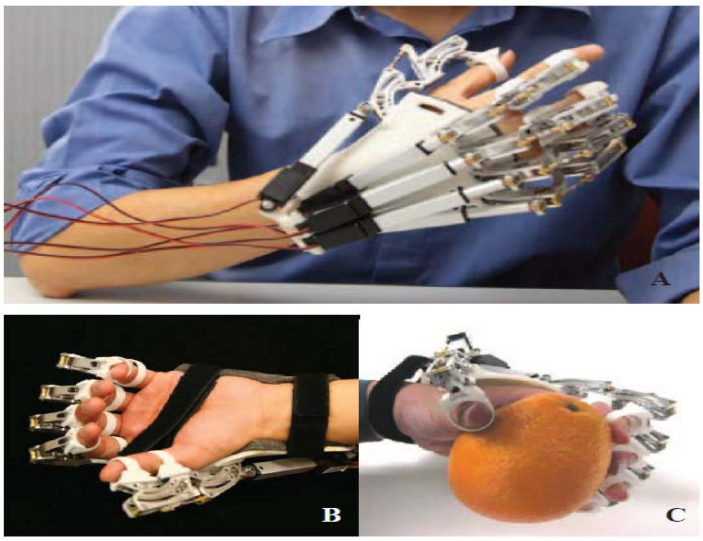

Fig. 1.12: Exoskeleton robotic hand training device in [35].

In addition, they proposed the EMG control strategy, which is using the EMG triggered training mode to control the function of hand opening and hand closing. The EMG triggered training mode shown in Fig. 1.13, which is consisting of hand closing triggering mode and hand opening triggering mode. Therefore, baseline and

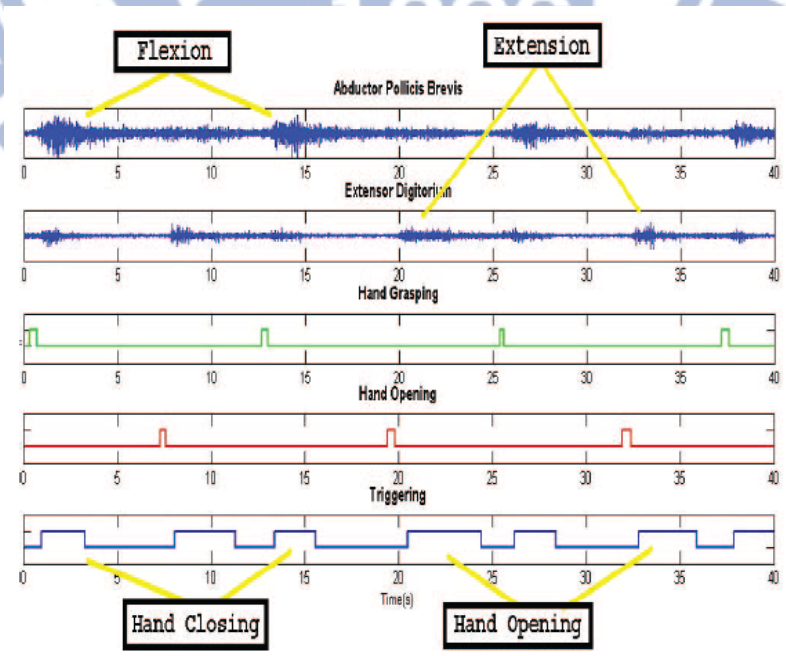

Fig. 1.13: EMG signals with EMG-triggered status in [35].

maximum voluntary contraction (MVC) of the EMG signals were measured at the beginning of each training session. The robotic system was running in a hand closing triggering mode if the EMG signals from the abductor pollicis brevis (APB) muscle exceeded the 20% of its MVC value. When it was running during a hand opening triggering mode, it would wait until the EMG signals from the extensor digitorum (ED) muscle exceeded the 20% of its MVC value before starting the hand opening action. This work used the muscle activation to control the robot hand, there was no feedback signal from the robot hand to evaluate the interaction between the robot hand and environmental.

In [36], the authors purposed a wearable hand robot (DULEX-II) that provides hand functioning for rehabilitation stroke survivors. In Fig. 1.14, DULEX-II consists of three degrees of freedom: one for wrist, one for index finger and one for combination of middle finger, a ring finger and a little finger. DULEX-II was actuated by three linear actuators: two electric linear motors for the finger and a double-acting pneumatic cylinder for the wrist. They used a data glove to control the movement of the robot hand, this is so-called self-motion control. The experiment results of finger position shows a 0.1mm error occurred when the length of the linear motor was changed from 2.5mm to 12.5mm from the target position, this would cause a finger angle error of about 0.45 degrees.

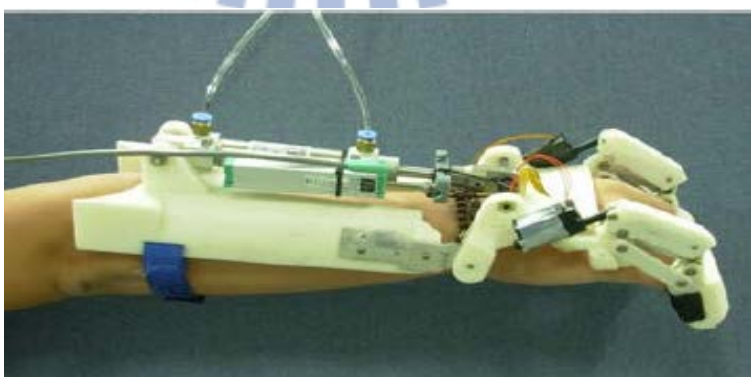

Fig. 1.14: The rehabilitation robotic hand, DULEX-II in [36].

From the literature reviews as previously mentioned, we summarize the features of rehabilitation hand exoskeleton is shown in Table 1.2. The various design criteria of hand exoskeleton such as actuator type, degrees of freedom (DOFs), power transmission and method of intention sense. The design criterion of hand exoskeleton is depends on the specific functions that needed, for example the use of sensor is essential for assistive hand exoskeleton to collect the user's motion intention and provide the motion assist for user.

Table 1.2: An overview of rehabilitation hand exoskeleton.

References	**Function**	**Actuator type**	**Degrees of freedom (DOF)**	**Power transmission**	**Method of intention sense**
Hasegawa et al.[31]	Assistive	Electric	11	Cable	EMG
Xing et al.[32]	Assistive/ rehabilitation	Pneumatic	2	Cable, linkage	N/A
Yamaura et al.[33]	Rehabilitation	Electric	2	Cable, linkage	Joint angles
Fu et al.[34]	Rehabilitation	Electric	2	Cable	FSR
Ho et al.[35]	Assistive/ rehabilitation	Electric	5	Linkage	EMG
Bae et al.[36]	Assistive/ rehabilitation	Electric & pneumatic	3	Linkage	Joint angles

1.4 Problem Definition

The demands of assistance and rehabilitation technologies are strong because of the population of stroke survivors is increasing yearly. The rehabilitation/assistance technologies play an important role for improving the quality of life for patients. Most of the researches focused on the interaction between the patients and robot hand technologies nevertheless the safety interaction of robot hand and environmental for patients is necessary for this inventions. In task-oriented training for grasping objects, we not only need to consider the human-robot interaction but also robot-environment interaction.

The purpose of this work is to develop a wearable hand exoskeleton to assist the stroke patients to complete the task training especially for grasping objects. In order to provide an excellent rehabilitation care, we need to make sure training procedures that are safe and comfortable. The details of statement are given as following:

1. Comfort in training:

Comfortable and convenient to wear robotic hand is very important. We must consider the weight of the robotic hand and intention control to ensure patients feel comfortable.

2. Concept of safety:

The rehabilitation robotic hand is designed for the stroke survivors and safety problems must be taken into consideration. We must consider how to generate an appropriate grasping force in order to assist the patients during training.

II. Mechanism Design of the Hand Exoskeleton

The objectives of this thesis is to design a wearable robotic hand for assisting the stroke patients to achieve the task oriented training. We suggest a control strategy to ensure the patients' comfort and safety in the training procedure. The developed mechanism of hand exoskeleton is shown in Fig. 2.1, which provides three degrees of freedom: one for thumb and two for index finger. The hand exoskeleton is actuated by three linear motors which attached on the back of the palm. The implementation of control system hardware architecture is shown in Fig. 2.2. It consists of linear motors, motor control boards, Arduino controller, force sensors circuit and buzzer.

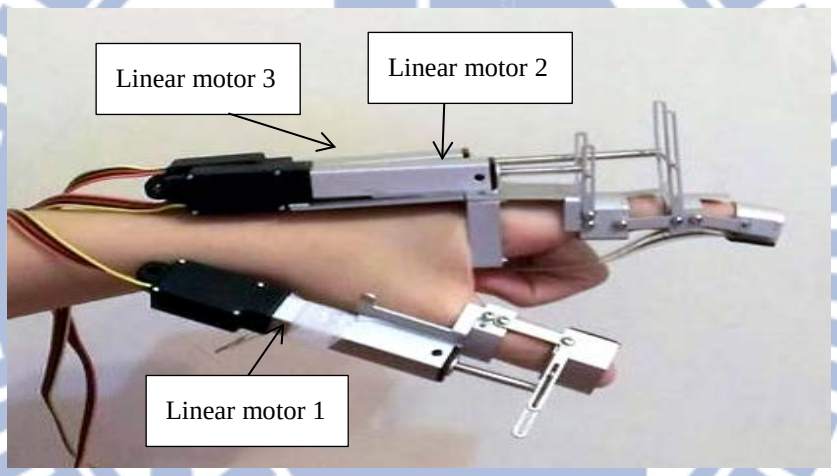

Fig. 2.1: A photo of the developed hand exoskeleton.

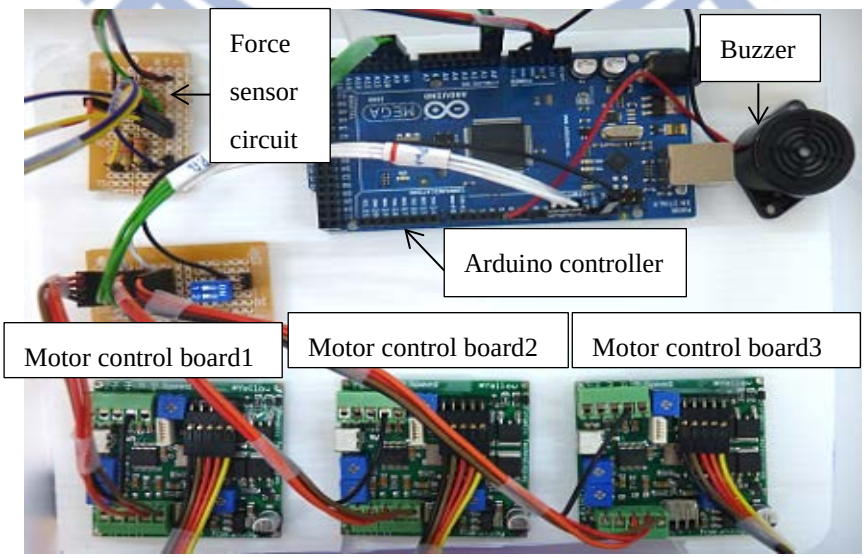

Fig. 2.2: The control system hardware.

In this chapter, the details of mechanism design of hand exoskeleton and hardware system will be described.

2.1 Degree of Freedom of Hand Exoskeleton

The robot can achieve different tasks with sufficient degrees of freedom (DOFs). The number of degrees of freedom is an important factor for a hand exoskeleton. If the number of degrees of freedom is inadequate, the movement of robot hand will be inflexible and constrained. Conversely, excessive number of degrees of freedom, the robot is difficult to control because of complex computation and the mechanism design will become harder.

In this thesis, we designed a hand exoskeleton which provides flexible movement and is capable to complete the task oriented training specifically for grasping objects. The hand exoskeleton consist of 3 DOF, 1 DOF, for thumb (IP) and 2 DOF, for index finger (MCP, PIP & DIP). The degree of freedom of hand exoskeleton is shown in Fig. 2.3.

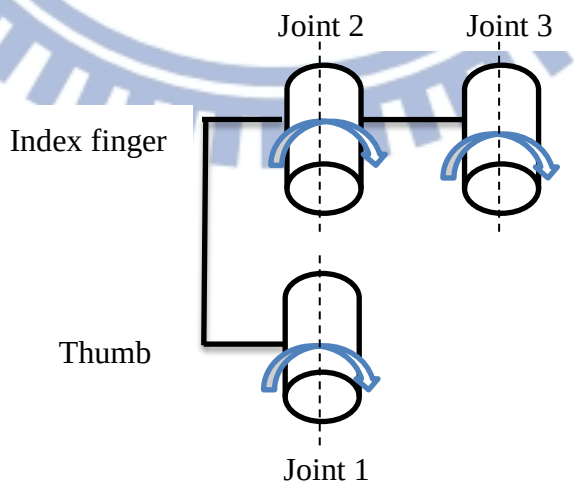

Fig. 2.3: The degree of freedom of hand exoskeleton.

2.2 The Range of Motion of the Exoskeleton Joint

Consider the wearable safety problem, the range of motion of finger exoskeleton joints should not exceed the excursion limit, for instance if the range of motion of exoskeleton joint exceeds the normal range of motion finger, it might cause injuries to the user. Therefore, we need to design the desired range of motion to ensure the user safety during the training process. The geometric mechanism structure is shown in Fig. 2.4. In this figure, there is a part of finger which contains two phalanges. Firstly, we define the base frame's origin point at O which is moved to the end point of the actuator when it fully retracts. When the actuator fully extends, the end is at Z. Z axis represents the length of actuator's stroke. The actuator is attached on the first phalange that provides a driving force to the slot slider (Y axis). Y axis represents the length of slot slider, which is symmetric attached beside the other phalange and important for constraint the motion of the phalange.

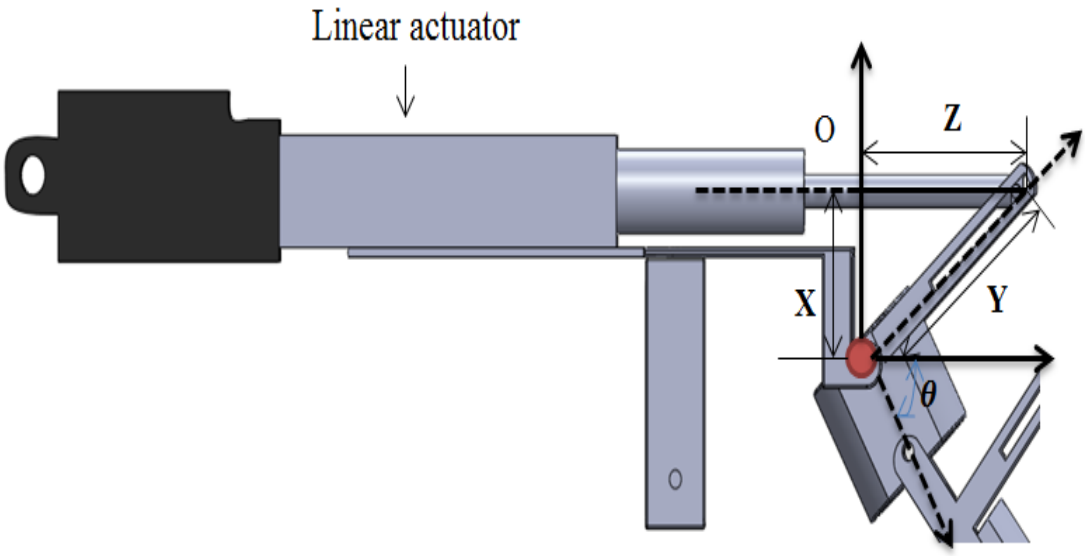

Fig. 2.4: Geometry definition of the mechanism structure.

We assume the desired range of finger joint motion is θ when the actuator retracts. Since we have the desired range of finger joint motion, we can design the distance between pivot point and actuator by equation (2.1).

$$X = \mathrm{Z} \cdot \tan\theta \tag{2.1}$$

Hence, the length of slot slider can be written as

$$Y = \sqrt{Z^2 + X^2} \tag{2.2}$$

Where X denotes the distance between pivot point and actuator,

Z is the length of actuator's stroke.

2.3 Mechanical Structure of Finger Exoskeleton

In this study, we design the wearable robotic fingers to assist stroke survivors to achieve the task oriented training for grasping object. We choose the aluminum alloy as the structural material. Aluminum alloy have been widely used as an engineering structures in many industries. The aluminum alloys are very light metal and high strength-to-weight ratio.

The wearable robotic fingers have two active joints for the index finger and one active joint for the thumb. We use linear motors to directly drive the motions of finger exoskeleton without any transmissions thus minimize the position error and provide a steady force. In addition, all of the linear actuators are attached on the back of the palm. From Fig. 2.5 to Fig. 2.7 shows the drawing of the hand exoskeleton. The index finger exoskeleton is actuated by two linear actuators shown in Fig. 2.5 and the thumb

exoskeleton is actuated by a single linear actuator shown in Fig. 2.6. Fig. 2.7 shows the assembly drawing of the hand exoskeleton. We also designed a slot slider which is symmetric attached on each phalange, the benefit of the slot slider is it able to constraint the motion of the phalange to ensure for the users safety.

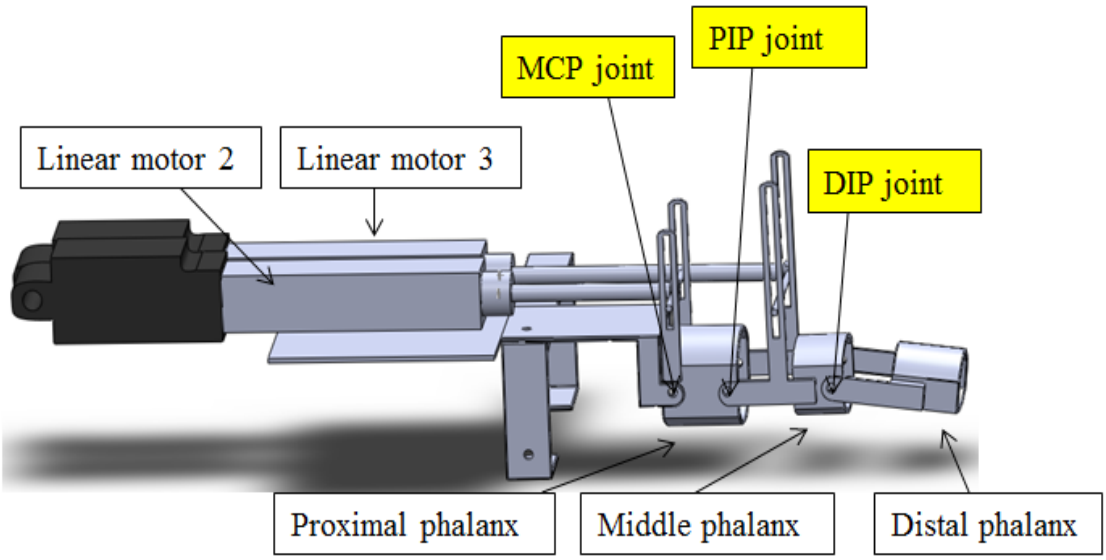

Fig. 2.5: The drawing of the index finger exoskeleton.

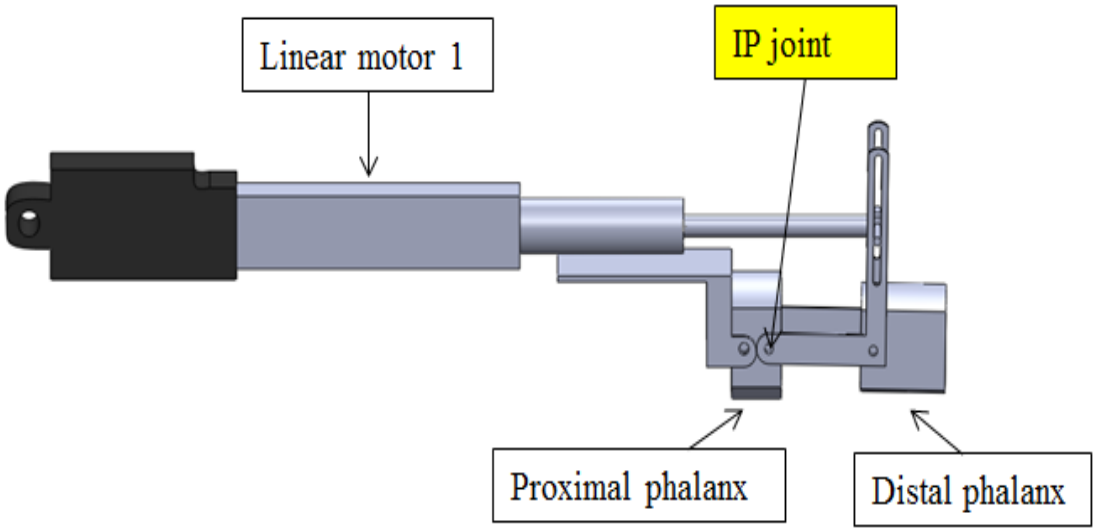

Fig. 2.6: The drawing of the thumb exoskeleton.

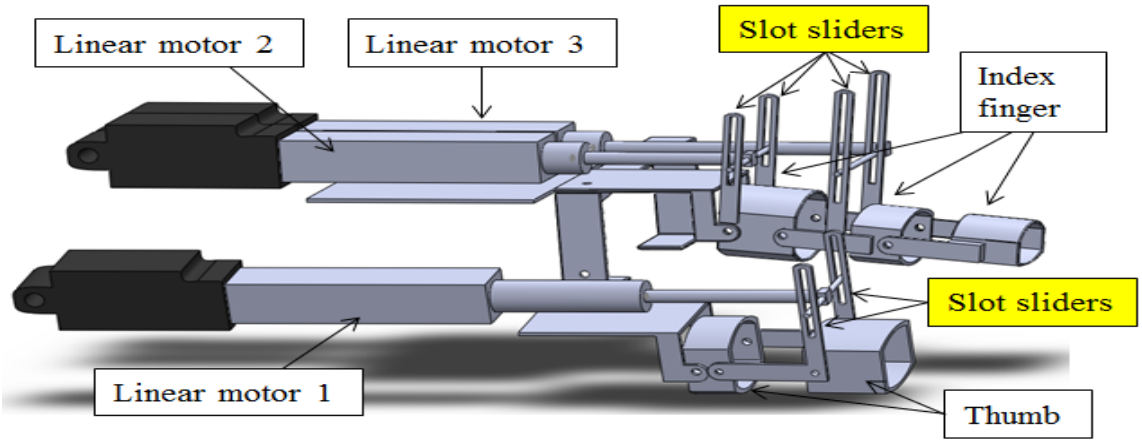

Fig. 2.7: The assembly drawing of the hand exoskeleton.

2.4 Hardware System Architecture

The control system hardware is shown in Fig. 2.8. It is composed of several blocks: linear motor, motor control board, Arduino controller, force sensors, buzzer and personal computer (PC). Considering safety and comfortable problem, we use two force sensors mounted on both inside and outside of each finger of the exoskeleton as shown in Fig. 2.9. The inside force sensor is used to detect the user's finger pressing force. The pressing force is measured to infer the user's intention of grasping motion. A compliance motion controller is then employed to generate the assist motion of the finger exoskeleton. Another one at outside is used to detect the contact force from the object to make sure the assistive grasping operation is achieved. A compliance motion controller is used to control the desirable grasping force to grasp the object successfully. Besides, the hand exoskeleton is actuated by three linear motors. We also design a graphical user interface (GUI) using LabView is shown in Fig. 2.10 that allows the physical therapist to choose the task program in PC. The controller's input signal are force feedback signal and position feedback signal from the force sensors and potentiometers respectively. Besides, the controller's output signals are pulse-width modulation (PWM) command signals to control the position

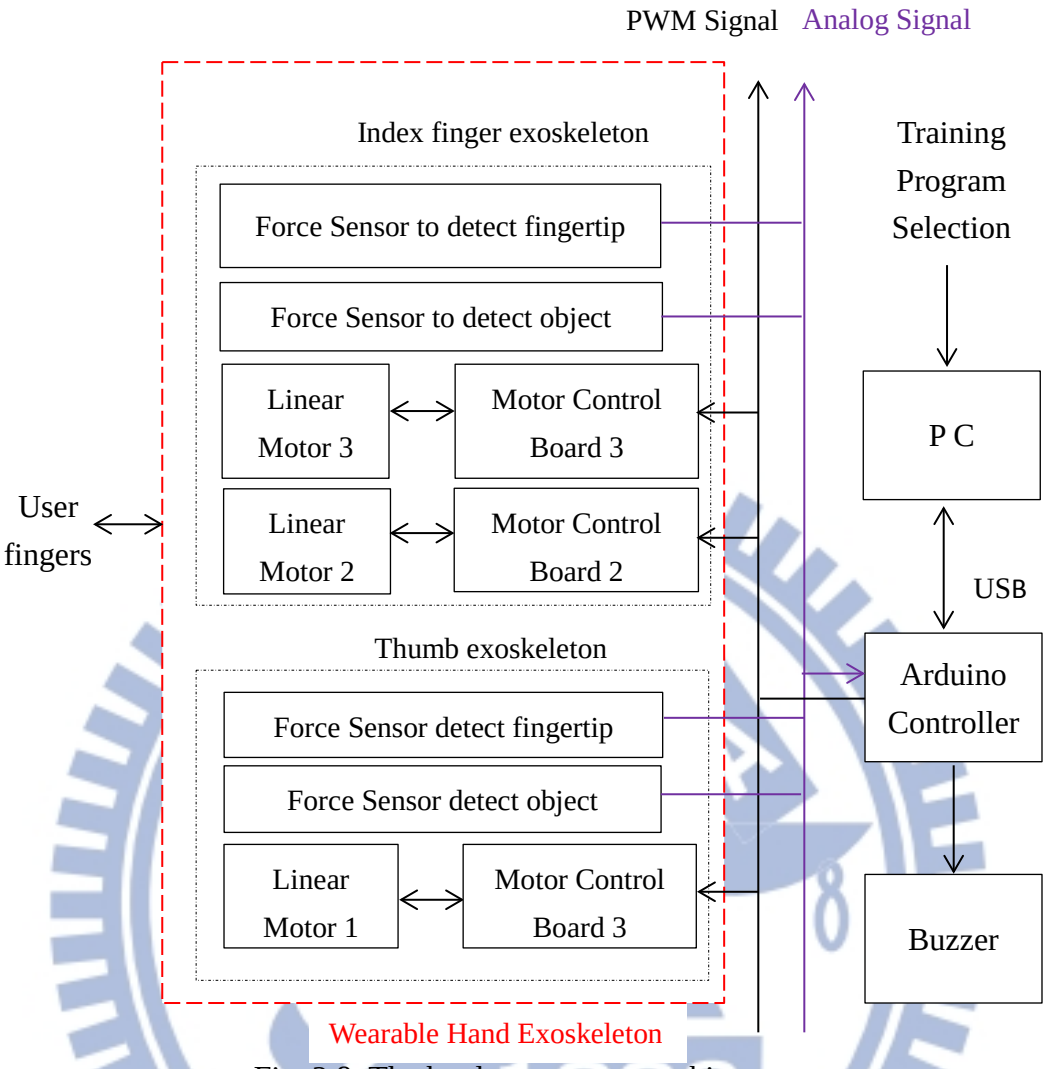

Fig. 2.8: The hardware system architecture.

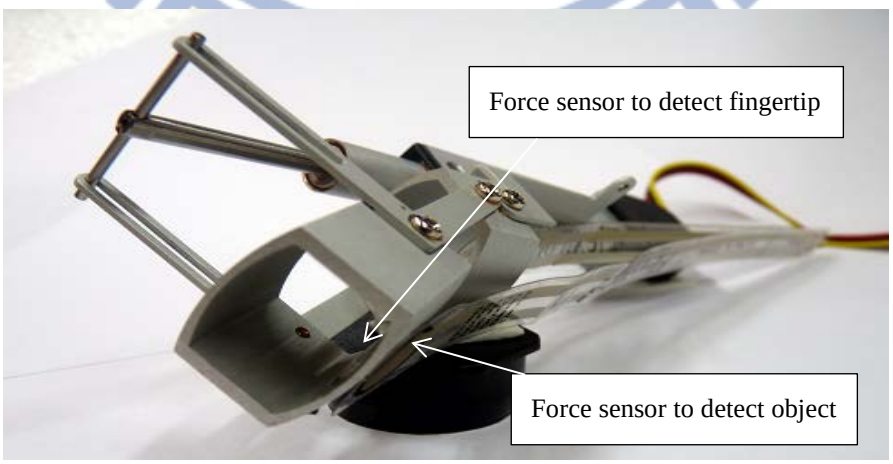

Fig. 2.9: Force sensors to detect separately the fingertip and object.

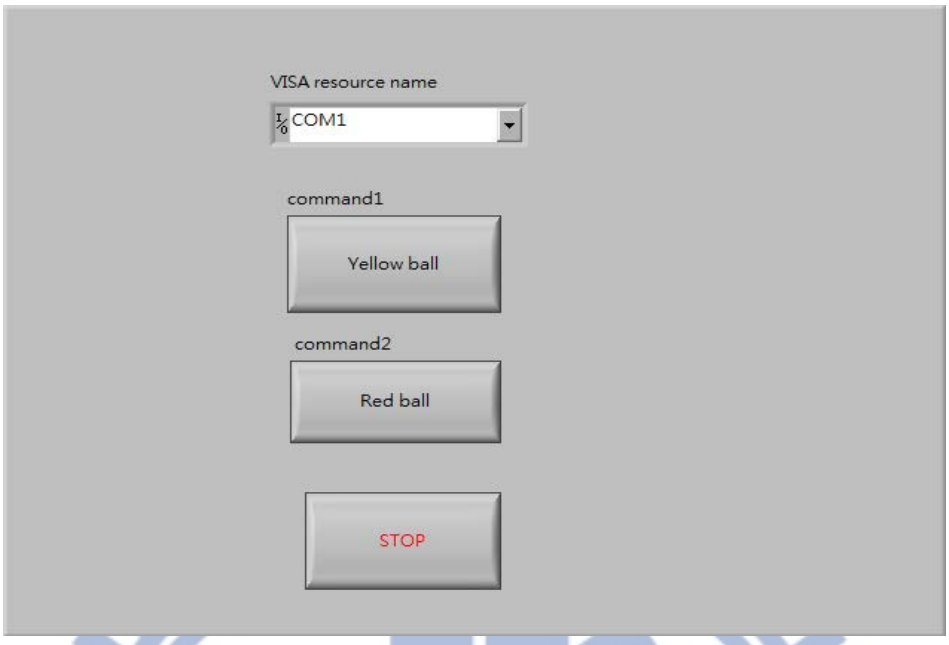

Fig. 2.10: The design of graphical user interface (GUI).

of the linear motors and buzzer signal is used to give a prompt when the grasping force is reached.

2.4.1 Controller

In this thesis, we use Arduino Mega 2560 as the embedded controller because of its small size, low cost and available for extension by users, it is very suitable for such robotic applications. The Arduino Mega 2560 in Fig. 2.11 is an open-source electronics prototyping platform which is based on the ATmega2560. The pin configurations of ATmega2560 is shown in Fig. 2.12. It has 54 digital input/output pins (of which 14 can be used as PWM outputs), 16 analog inputs, 4 UARTs (hardware serial ports), a 16 MHz crystal oscillator, a USB connection, a power jack, an ICSP header, and a reset button. The characteristics of Arduino Mega 2560 are shown in Table 2.1. The Arduino software consists of a development environment (IDE) and the core libraries that can be runs on Windows, Mac OS X and Linux. The core libraries are written in C and C++ and compiled using avr-gcc and AVR Libc.

Fig. 2.11: The Arduino Mega 2560 board.

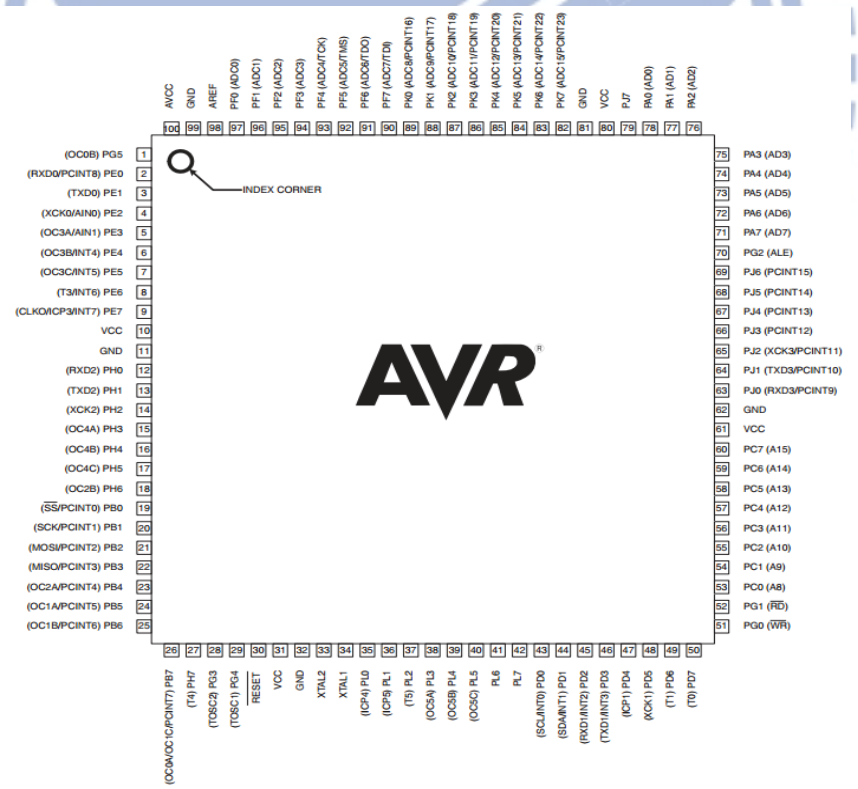

Fig. 2.12: The pin configurations of ATmega2560 in [37].

Table 2.1: The characteristics of Arduino Mega 2560 in [37]:

Microcontroller	ATmega2560
Operating Voltage	5 V
Input Voltage(recommended)	7-12 V
Input Voltage(limits)	6-20 V
Digital I/O Pins	54 of which 14 provide PWM output
Analog Input Pins	16
DC Current per I/O Pin	40 mA
DC Current for 3.3V Pin	50 mA
Flash Memory	256 KB of which 8KB used by boot loader
SRAM	8 KB
EEPROM	4 KB
Clock Speed	16 MHZ

2.4.2 Actuator

We choose the L12-P linear actuator produced by Firgelli Technologies Inc. to drive the robotic fingers in this thesis. L12-P linear actuator as shown in Fig. 2.13

consists of a Permanent Magnet DC (PMDC) motor, an internal potentiometer and a gear reduction. It has an internal potentiometer that can be used to provide position feedback and we can choose the gear ratio depend on force or speed needed. The load curve of the gear reduction and the specifications of L12-P as shown in Fig. 2.14 and Table 2.2, respectively. In addition, the benefits of this actuator are low voltage, compact miniature size and equal push/pull force. It also very light weight and easy to mount on the human hand.

Fig. 2.13: The linear actuator L12-P.

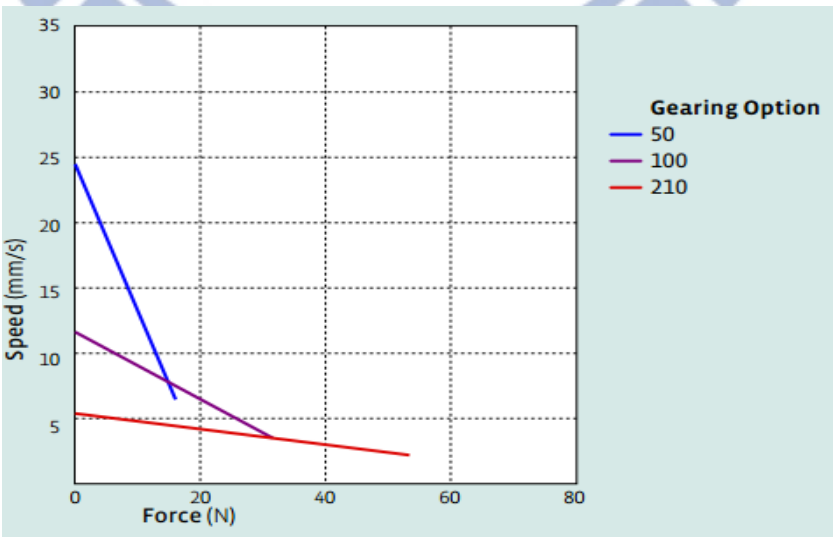

Fig. 2.14: The load curve of the gear reduction in [38].

Table 2.2: The specifications of L12-P in [38].

Gear ratio	**100**
Peak power point	23N - 6 mm/s
Peak efficient point	12N - 8 mm/s
Max speed (no load)	12 mm/s
Backdrive Force	80 N
Stroke	**50 mm**
Weight	40 g
Positional accuracy	0.2 mm
Max side force (fully extended)	30 N
Operating voltage	12 V
Duty cycle	20 %
Operating temperature	-10 ℃ to 50 ℃
Feedback potentiometer	2.75 kΩ/mm ± 30 %, 1 % linearity
Stall current	200 mA
Audible noise	55 dB at 45 cm

In the part of motor control, we utilize the linear actuator control (LAC) board produced by Firgelli Technologies Inc.. The LAC Board is a stand-alone closed-loop control board specifically designed for Firgelli "P" series actuators. It supported input signals include USB, Voltage, Current, RC Servo, and PWM. It is also available for on board adjustment of speed, sensitivity, and stroke limits. Each LAC Board controls one linear actuator which required an external power supply rated for the actuator. We can derive the position feedback signal from potentiometer through the LAC board and estimate the error. The LAC board is shown in Fig. 2.15 and the specifications of LAC board as shown in Table 2.3.

Fig. 2.15: The LAC board.

Table 2.3: The specifications of LAC board in [39].

Control input modes	Digital: USB, RC Servo, 1kHz PWM Analog: 0-3.3 V, 4-20 mA
Controller	10-bit Dual Sample Rate Quasi PD
Dimensions	50 mm × 50 mm
Power	5-24 VDC, 4 Amps peak current at 10 % duty cycle
Operating environment	-10 ℃ to 50 ℃ at 10-80 % relative humidity

2.4.3 Measurement of joint motion

In this section, we measure the angles of each finger exoskeleton joints for

kinematic analysis. In the experiments, we give a command to push the linear motor to a specific position and measure angles of finger exoskeleton by a protractor. The relationship between displacement of linear motor and angle of finger joint is shown as Fig 2.16. In Fig. 2.17, we use the curve fitting to obtain equations of approximating curve to the raw data by MATLAB, which are expressed in (2.3)~(2.5)

$$\theta_{mcp} = -1.954x^4 + 11.521x^3 + -19.762x^2 + 35.731\text{x} - 0.142 \quad (2.3)$$

$$\theta_{pip} = -0.576x^4 + 4.546x^3 - 10.891x^2 + 31.478\text{x} - 0.177 \quad (2.4)$$

$$\theta_{ip} = -2.979x^4 + 16.222x^3 - 26.831x^2 + 41.867\text{x} - 0.455 \quad (2.5)$$

where θ_{mcp} is MCP joint of index finger exoskeleton, θ_{pip} is PIP joint of index finger exoskeleton, θ_{ip} is IP joint of thumb exoskeleton and x is the displacement of linear motor.

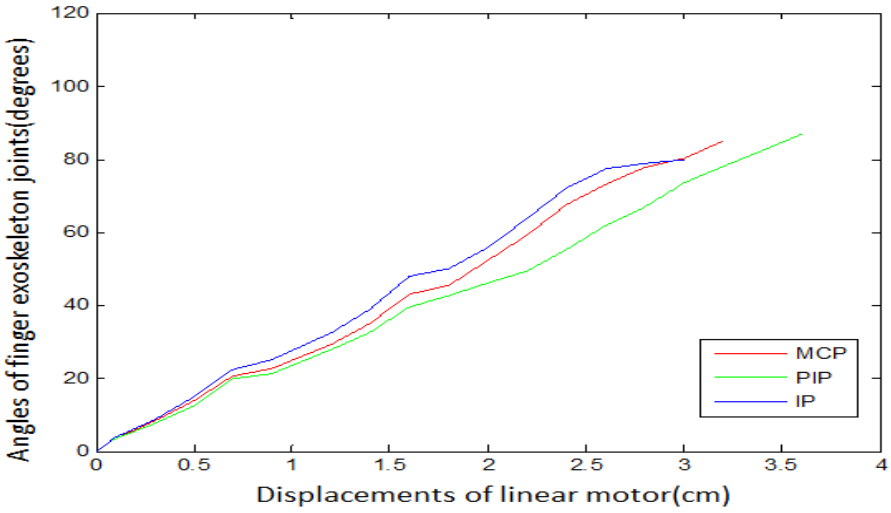

Fig 2.16: The relationship between displacements of linear motor and angles of finger exoskeleton (experiment result).

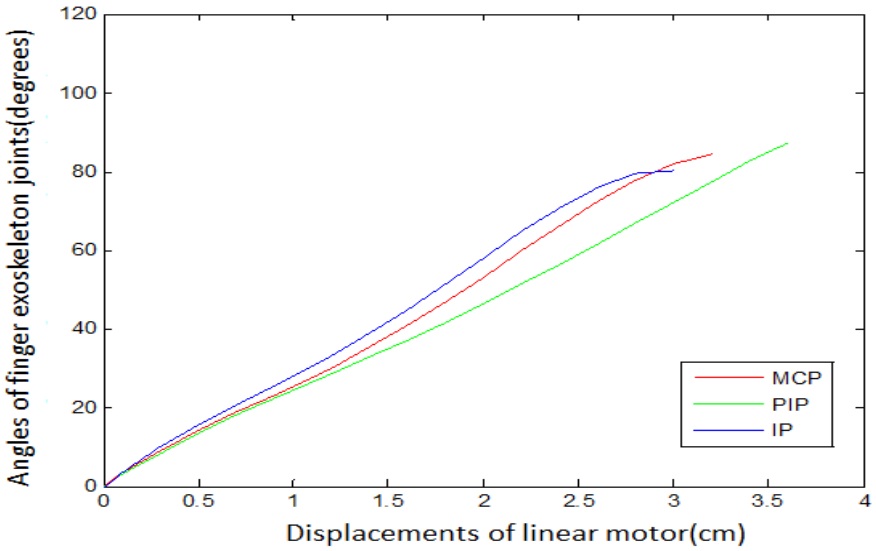

Fig 2.17: The relationship between displacements of linear motor and angles of finger exoskeleton (calibration result).

2.4.4 Force Sensor

In this thesis, we utilize the FlexiForce force sensitive resistance (FSR) sensor developed by Tekscan to detect the force. The FlexiForce sensor can be easily integrated with its paper-thin construction, flexibility and force measurement ability. This sensor is ideal for our research because it can measure both static and dynamic forces between almost any two surfaces without disturbance. The FlexiForce sensor and the specifications of the sensor are shown in Fig. 2.18 and Table 2.4 respectively.

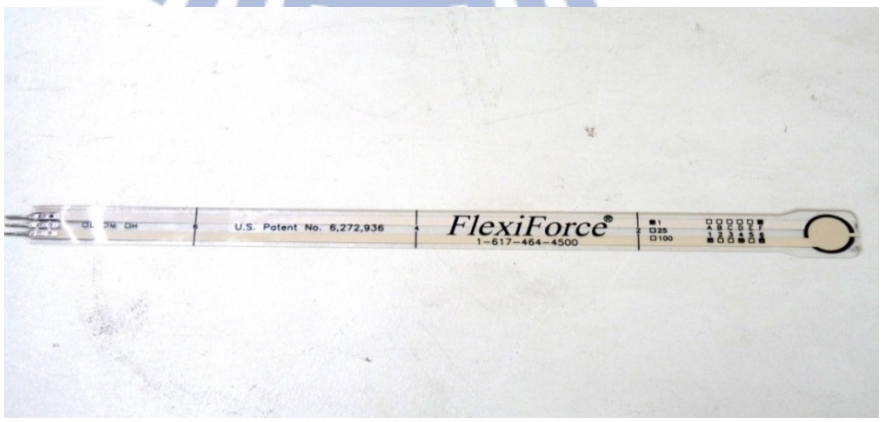

Fig. 2.18: The FlexiForce sensor model A201.

Table 2.4: The specifications of FlexiForce sensor in [40].

Model	A201
Thickness	0.208 mm
Length	102 mm
Width	14 mm
Sensing area	9.53 mm diameter
Force range	1 lb
Linearity (error)	< ± 3 %
Response time	< ± 5 μsec
Repeatability	< ± 2.5 % of full scale
Hysteresis	< 4.5 % of full scale
Drift	< 5 % per logarithmic time scale
Operating temperature	-9 ℃ to 60 ℃

2.4.5 Force Calibration

In order to improve the accuracy of force sensing, a calibration test is needed before using it in grasping tasks. In this experiment, we test eleven different stainless steel weights (1g, 2g, 5g, 10g, 20g, 50g, 100g, 200g, 300g, 400g, 450g) individually. Firstly, we place the Flexiforce sensor (1 lbs) on the table. Later, we put down the weight on the Flexiforce sensor to read the data from the Arduino controller. Fig. 2.19 is the principle drawing of the force calibration and Fig. 2.20 is the experiment results

of the force calibration. We use the curve fitting to obtain an equation of approximating curve to the raw data by MATLAB. The equation of force calibration can be expressed in (2.6)

$$Y = 0.00000000018x^4 - 0.00000016x^3 + 0.000058x^2 - 0.0017x + 0.0267 \quad (2.6)$$

where Y is force in N and x is the gray code data.

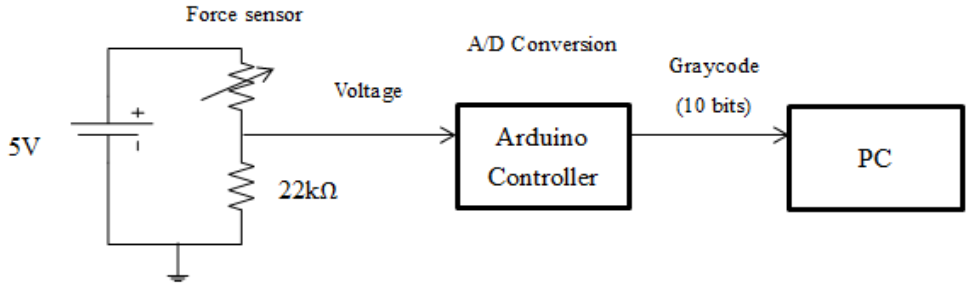

Fig. 2.19: The principle drawing of the force calibration.

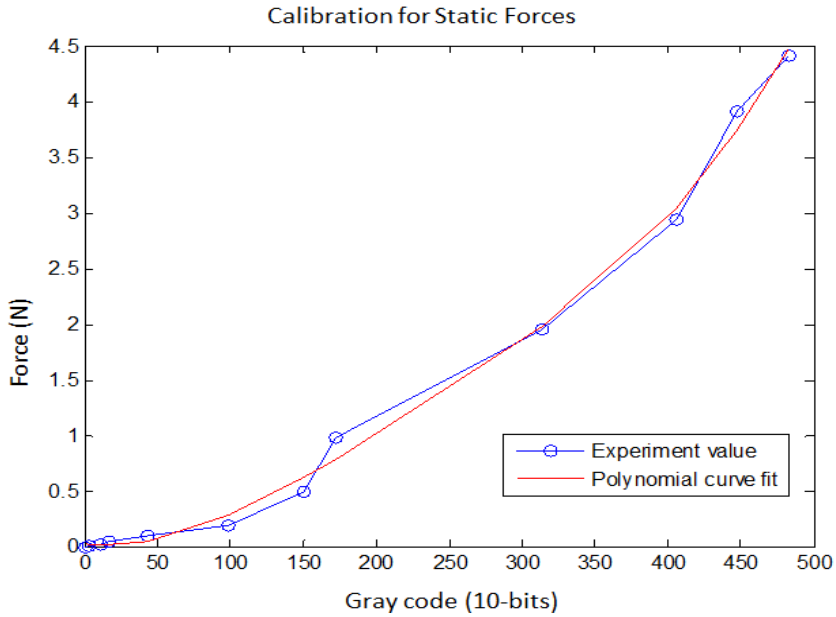

Fig. 2.20: The experiment results of force calibration.

III. Kinematic Analysis of Two-Finger Exoskeleton

Kinematic is the science of motion that refers to geometric variation depending on time, including the position, velocity, the acceleration, etc. Robot kinematics is mainly classified into two types: forward kinematics and inverse kinematics. In this chapter, the forward kinematics and inverse kinematics are derived in the paragraphs.

3.1 Forward Kinematic Analysis

Forward kinematics is also known as direct kinematics. The forward kinematics is to determine the position and orientation of the end-effector by given the values for the joint variables of the robot. The Denavit-Hartenberg, or D-H convention is common used for selecting frames of reference in robotic applications. In this method, coordinate frame is attached to each link, and create the table of link parameters referred to the relationship of the rotation and translation between these coordinates. Also, the homogeneous transformations matrices are used to describe the relative position or orientation of these frames. The D-H parameters representation for a rotational joint is shown in Fig. 3.1, which is defined as follows [41]:

- Assign the $\hat{Z}_i$ axis pointing along the *i*th joint axis.
- Assign the $\hat{X}_i$ axis pointing along the common perpendicular, or, if the axes intersect, assign $\hat{X}_i$ to be normal to the plane containing the two axes.
- Assign the $\hat{Y}_i$ axis to complete a right-hand coordinate system.
- a_i denotes the distance from $\hat{Z}_i$ to $\hat{Z}_{i+1}$ measured along $\hat{X}_i$.
- α_i denotes the angle from $\hat{Z}_i$ to $\hat{Z}_{i+1}$ measured about $\hat{X}_i$.
- d_i denotes the distance from $\hat{X}_{i-1}$ to $\hat{X}_1$ measured along $\hat{Z}_i$.
- θ_i denotes the angle from $\hat{X}_{i-1}$ to $\hat{X}_1$ measured about $\hat{Z}_i$.

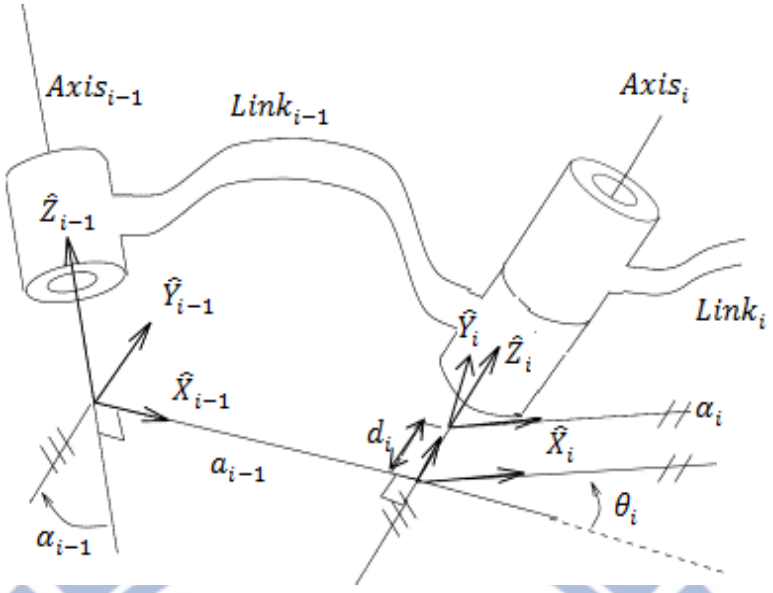

Fig. 3.1: D-H parameters representation for a rotational joint.

In D-H convention, the general homogeneous transformation ${}^{i-1}_{i}T$ is represented in equation (3.1), which contains of link length, link twist, link offset and joint angle associated with link i and joint i, these four parameters are a_i, α_i, d_i and θ_i, respectively.

$$ {}^{i-1}_{i}T = \begin{bmatrix} cos\theta_i & -sin\theta_i & 0 & a_{i-1} \\ sin\theta_i cos\alpha_{i-1} & cos\theta_i cos\alpha_{i-1} & -sin\alpha_{i-1} & -sin\alpha_{i-1} d_i \\ sin\theta_i sin\alpha_{i-1} & cos\theta_i sin\alpha_{i-1} & cos\alpha_{i-1} & cos\alpha_{i-1} d_i \\ 0 & 0 & 0 & 1 \end{bmatrix} \quad (3.1) $$

3.1.1 Forward Kinematics for Index Finger

The hand exoskeleton of index finger is designed by two active joints which contain MCP, the PIP and DIP joints that are coupled together. The joint of each link of our hand exoskeleton is a frame to determine the kinematic derivation, as shown in Fig. 3.2. Firstly, we define the base frame's origin point at O and subsequent frames are defined by D-H convention. After that we can find out each coordinate parameter in Table. 3.1.

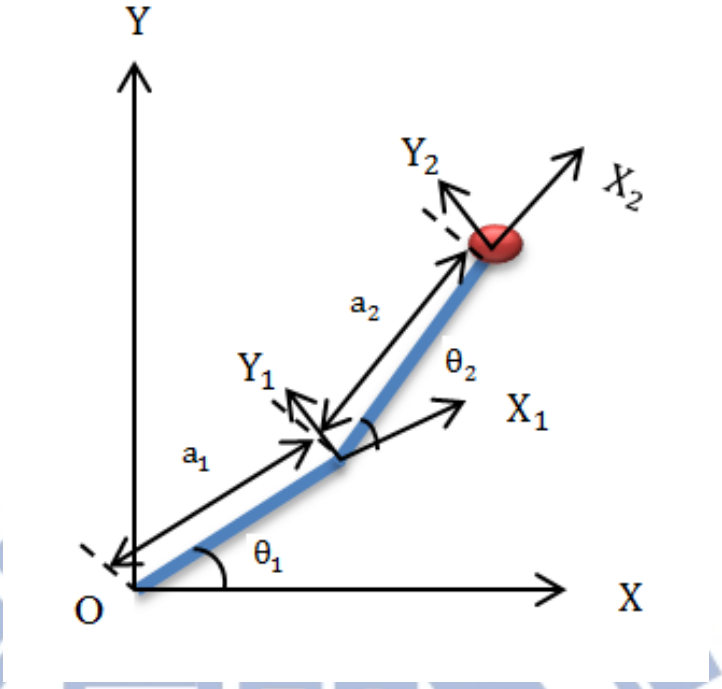

Fig. 3.2: Link-frame assignments of index finger.

Table. 3.1: D-H parameters of index finger.

i	a_{i-1}	α_{i-1}	d_i	θ_i
1	0	0	0	θ_1
2	a_1 (MCP)	0	0	θ_2
3	a_2 (PIP&DIP)	0	0	0

Substituting the D-H parameters into equation (3.1), the homogeneous transformation matrices (3.2) ~ (3.4) can be obtained.

$$ {}^{0}_{1}T = \begin{bmatrix} cos\theta_1 & -sin\theta_1 & 0 & 0 \\ sin\theta_1 & cos\theta_1 & 0 & 0 \\ 0 & 0 & 1 & 0 \\ 0 & 0 & 0 & 1 \end{bmatrix} \quad (3.2) $$

$$ {}^{1}_{2}T = \begin{bmatrix} cos\theta_2 & -sin\theta_2 & 0 & a_1 \\ sin\theta_2 & cos\theta_2 & 0 & 0 \\ 0 & 0 & 1 & 0 \\ 0 & 0 & 0 & 1 \end{bmatrix} \tag{3.3} $$

$$ {}^{2}_{3}T = \begin{bmatrix} 1 & 0 & 0 & a_2 \\ 0 & 1 & 0 & 0 \\ 0 & 0 & 1 & 0 \\ 0 & 0 & 0 & 1 \end{bmatrix} \tag{3.4} $$

Hence, the forward kinematics for the hand exoskeleton of index finger is given by:

$$ {}^{0}_{3}T = {}^{0}_{1}T \times {}^{1}_{2}T \times {}^{2}_{3}T $$

$$ = \begin{bmatrix} c_{12} & -s_{12} & 0 & a_1c_1 + a_2c_{12} \\ s_{12} & c_{12} & 0 & a_1s_1 + a_2s_{12} \\ 0 & 0 & 1 & 0 \\ 0 & 0 & 0 & 1 \end{bmatrix} \tag{3.5} $$

Where

$c_{12} = \cos\theta_1 \cos\theta_2 - \sin\theta_1 \sin\theta_2$ and

$s_{12} = \sin\theta_1 \cos\theta_2 + \cos\theta_1 \sin\theta_2$

3.1.2 Forward Kinematics for Thumb

The hand exoskeleton of thumb is contains MCP and IP joint. In this thesis, we only control the IP joint. The joint of each link of our hand exoskeleton is a frame to determine the kinematic derivation, as shown in Fig. 3.3. Firstly, we define the base frame's origin point at O and subsequent frames are defined by D-H convention. After that, we can find out each coordinate parameter in Table. 3.2.

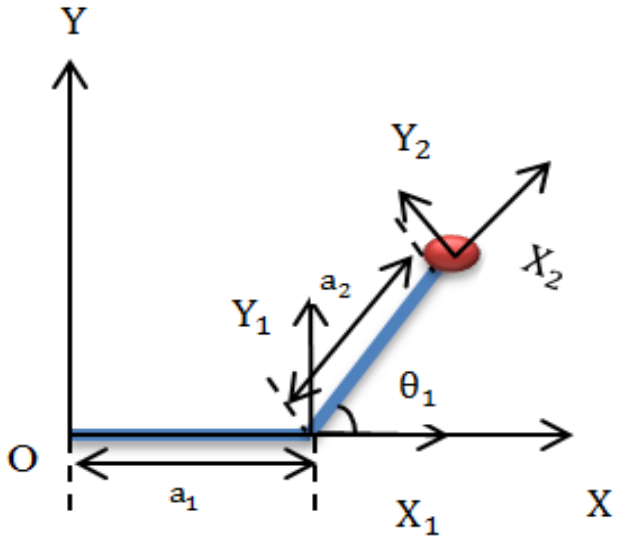

Fig. 3.3: Link-frame assignments of thumb.

Table. 3.2: D-H parameters of thumb.

i	a_{i-1}	α_{i-1}	d_i	θ_i
1	0	0	0	0
2	a_1 (MCP)	0	0	0
3	a_2 (IP)	0	0	θ_1

Substituting the D-H parameters into equation (3.1), the homogeneous transformation matrices (3.6) ~ (3.8) can be obtained.

$$ {}^{0}_{1}T = \begin{bmatrix} 1 & 0 & 0 & 0 \\ 0 & 1 & 0 & 0 \\ 0 & 0 & 1 & 0 \\ 0 & 0 & 0 & 1 \end{bmatrix} \tag{3.6} $$

$$ {}^{1}_{2}T = \begin{bmatrix} 1 & 0 & 0 & a_1 \\ 0 & 1 & 0 & 0 \\ 0 & 0 & 1 & 0 \\ 0 & 0 & 0 & 1 \end{bmatrix} \tag{3.7} $$

$$ {}^{2}_{3}T = \begin{bmatrix} cos\theta_1 & -sin\theta_1 & 0 & a_2 \\ sin\theta_1 & cos\theta_1 & 0 & 0 \\ 0 & 0 & 1 & 0 \\ 0 & 0 & 0 & 1 \end{bmatrix} \quad (3.8) $$

Hence, the forward kinematic for the hand exoskeleton of index finger is given by:

$$ {}^{0}_{3}T = {}^{0}_{1}T \times {}^{1}_{2}T \times {}^{2}_{3}T $$

$$ = \begin{bmatrix} cos\theta_1 & -sin\theta_1 & 0 & a_1a_2cos\theta_1 \\ sin\theta_1 & cos\theta_1 & 0 & a_1sin\theta_1 \\ 0 & 0 & 1 & 0 \\ 0 & 0 & 0 & 1 \end{bmatrix} \quad (3.9) $$

3.2 Inverse Kinematics Analysis

3.2.1 Inverse Kinematics for Index Finger

In inverse kinematics, the length of each link and end-effector location is given and we have to calculate the angle of each joint. They are detailed below:

1. By using the previous forward kinematics homogenous matrices (3.5), we assume that,

$$ {}^{B}_{W}T = {}^{0}_{3}T = \begin{bmatrix} c_{12} & -s_{12} & 0 & a_1c_1 + a_2c_{12} \\ s_{12} & c_{12} & 0 & a_1s_1 + a_2s_{12} \\ 0 & 0 & 1 & 0 \\ 0 & 0 & 0 & 1 \end{bmatrix} = \begin{bmatrix} n_x & o_x & a_x & p_x \\ n_y & o_y & a_y & p_y \\ n_z & o_z & a_z & p_z \\ 0 & 0 & 0 & 1 \end{bmatrix} \quad (3.10) $$

Then

$$ n_x = c_{12} \quad (3.11) $$

$$ n_y = s_{12} \quad (3.12) $$

$$p_x = a_1 c_1 + a_2 c_{12} \tag{3.13}$$

$$p_y = a_1 s_1 + a_2 s_{12} \tag{3.14}$$

2. Square both (3.13) and (3.14) and add them, we obtain

$$p_x{}^2 + p_y{}^2 = a_1{}^2 + a_2{}^2 + 2a_1 a_2 c_2 \tag{3.15}$$

Hence

$$\theta_2 = \cos^{-1}\left(\frac{p_x{}^2 + p_y{}^2 - a_1{}^2 - a_2{}^2}{2a_1 a_2}\right) \tag{3.16}$$

3. To find θ_1, let (3.13) divided by (3.14) can be written as

$$\frac{p_x}{p_y} = \frac{a_1 c_1 + a_2 c_{12}}{a_1 s_1 + a_2 s_{12}} \tag{3.17}$$

Solving (3.17) for θ_1, we obtain

$$\theta_1 = \tan^{-1}\left[\frac{-p_x(a_2 s_2) + p_y(a_1 + a_2 c_2)}{p_y(a_2 s_2) + p_x(a_1 + a_2 c_2)}\right] \tag{3.18}$$

3.2.2 Inverse Kinematics for Thumb

By using the previous forward kinematics homogenous matrices (3.9), we assume that,

$$ {}^{B}_{W}T = {}^{0}_{3}T = \begin{bmatrix} cos\theta_1 & -sin\theta_1 & 0 & a_1a_2cos\theta_1 \\ sin\theta_1 & cos\theta_1 & 0 & a_1sin\theta_1 \\ 0 & 0 & 1 & 0 \\ 0 & 0 & 0 & 1 \end{bmatrix} = \begin{bmatrix} n_x & o_x & a_x & p_x \\ n_y & o_y & a_y & p_y \\ n_z & o_z & a_z & p_z \\ 0 & 0 & 0 & 1 \end{bmatrix} \quad (3.19) $$

Then

$$ o_x = -sin\theta_1 \quad (3.20) $$

$$ o_y = cos\theta_1 \quad (3.21) $$

We obtain

$$ \theta_1 = \tan^{-1}\left(-\frac{o_x}{o_y}\right) \quad (3.22) $$

3.3 Discussion of Kinematic Analysis

In this thesis, we use Denavit-Hartenberg to determine the forward kinematics and inverse kinematics. This method reduces the parameters with only four parameter (a_i, α_i, d_i and θ_i) in transformation to describe the joints and position of links unambiguously. In inverse kinematics, we determine the joint coordinates to reach the desired position of end-effector. We obtain joint coordinates with given the desired Cartesian coordinates through inverse kinematic and able to let the robot fingers to move to the desired goal. In forward kinematic, we determine the position and orientation of robot fingers from the feedback angles of each exoskeleton joints to check if the desired position was reached.

IV. Compliance Control for Robotic Fingers

Most industrial robots are controlled in traditional way that allows to follow desired trajectories but the robots still cannot perform the contact tasks satisfactorily. It will become a barrier and directly threaten hand safety without force control. In this work, we propose the wearable rehabilitation robotic fingers to assist the stroke patients to achieve task oriented training specifically for grasping object. The robotic fingers provide a force sensing at the end-effector of robot hand in order to enhance patients safety in training procedure by using compliance control. In our control strategy, the end-effector of robot fingers with force sensor is modeled as a compliance control model. The system will execute the task by using the compliance model in two cases. Firstly, the robotic fingers perform compliance motion when human exert a force. Another case is the robot fingers detect a contact force from object and achieve the compliance motion. Compared with computed torque control, the compliance control simplified the dynamic system which can varies the stiffness of robot hand by tuning the physical parameters of compliance model. In this chapter, the compliance control system architecture will be proposed. After that, the compliance model and the simulation of compliance model will be presented.

4.1 Compliance Control System Architecture

The proposed compliance control system architecture for robot fingers composed of two blocks: user compliance control and grasping compliance control. The purpose of user compliance control is to allow the user control the movement easily with their intention and make him/herself feel comfortable. Fig. 4.1 is shown the system architecture of user compliance control. Consider to comfortable issue, a force sensor is mounted inside of fingers exoskeleton to collect the user's active force and check if

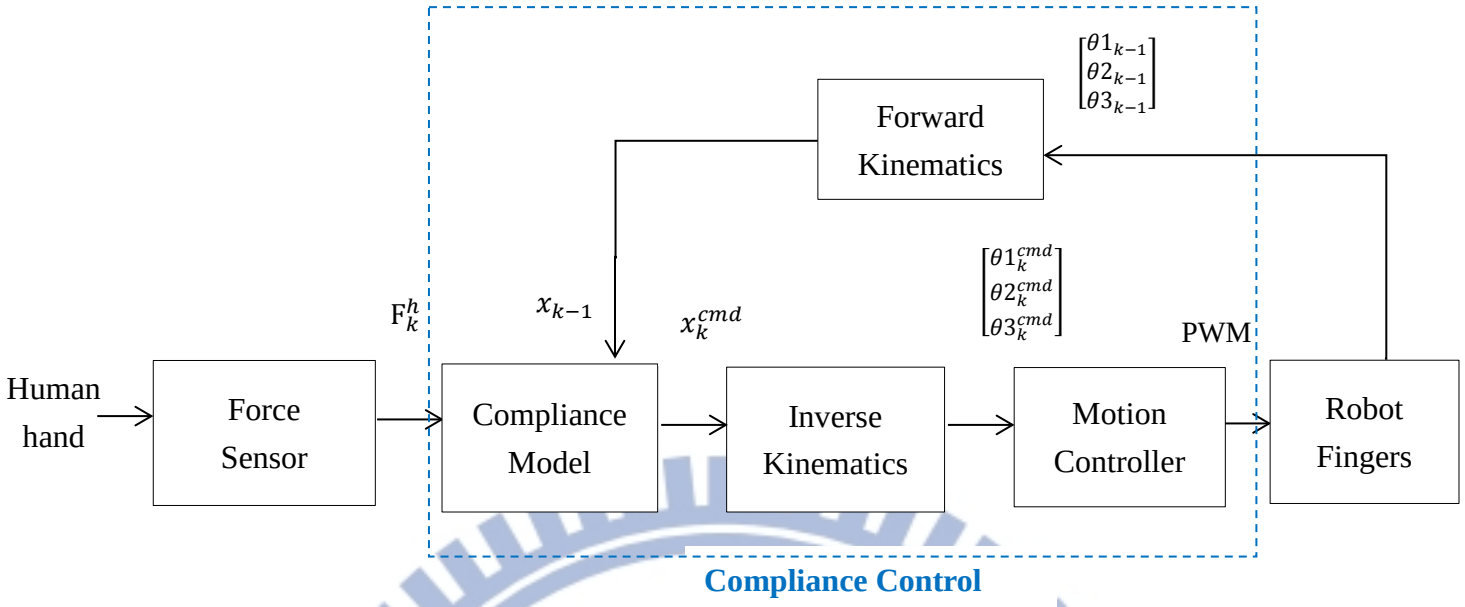

Fig. 4.1: System architecture of user compliance control.

the user's active force is exerted. If we use the position control without force sensing, the user might not be comfortable because they could not control the movement of hand exoskeleton by their intention. In user compliance control, the compliance model will calculate the displacement of x_k^{cmd} according to the finger pressing force F_k^h measured by force sensor. The inverse kinematic determines the joint angles according to the x_k^{cmd} and give a command to control the robot fingers joints and the potentiometers derived the actual joint angles and calculated the end-effector actual position via forward kinematic feedback to the compliance model at the same time.

In addition, the purpose of grasping compliance control is to provide an assistive grasping force when the hand exoskeleton contact with the object and help the patient to grasp the different weights of objects without damage in grasping task. The system architecture of grasping compliance control is shown in Fig. 4.2. Considering the safety grasping procedure for stroke patient to prevent injuries is necessary because of his/her hand is very vulnerable after a stroke. Therefore, we use a force sensor mounted outside of fingers exoskeleton to detect the contact force from object and

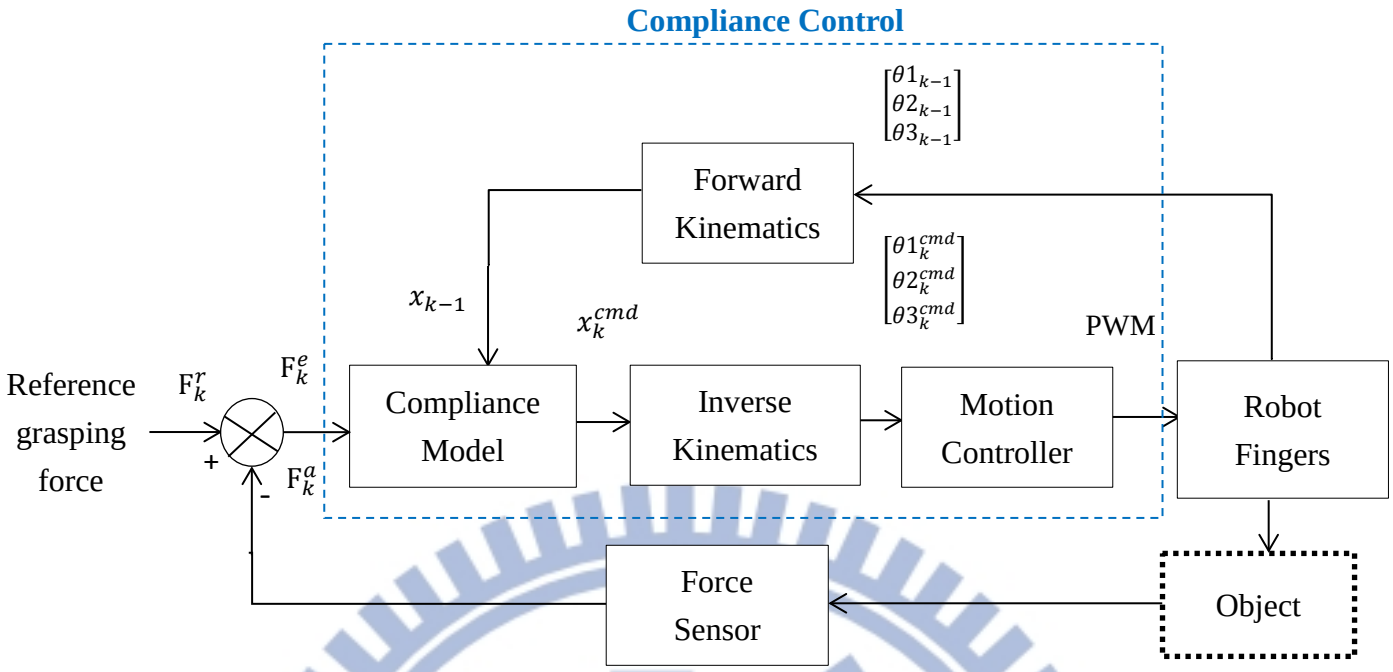

Fig. 4.2: System architecture of grasping compliance control.

make sure the assistive force is enough for each grasping task. In grasping compliance control, F_k^r is the reference grasping force we give, the compliance model will calculate the displacement x_k^{cmd}. Then, the inverse kinematic determines the joint angles according to the x_k^{cmd} and give a command to control the robot fingers joints. The potentiometers derived the actual joint angles and calculated the end-effector actual position via forward kinematic feedback to the compliance model. At the same time, the force sensors will measure the actual grasping force and compare with the references grasping force.

4.2 Compliance Model

In this thesis, we wish our robot fingers can mimic human hand when the robot fingers contact with the object or detect a human force. Therefore, we employ the compliance model as shown in Fig. 4.3. The compliance model is a mass-damper-spring system which consists of mass (M), damper (D) and spring (K). We can change the compliance level (stiffness) of the robot hand by tuning the physical parameters.

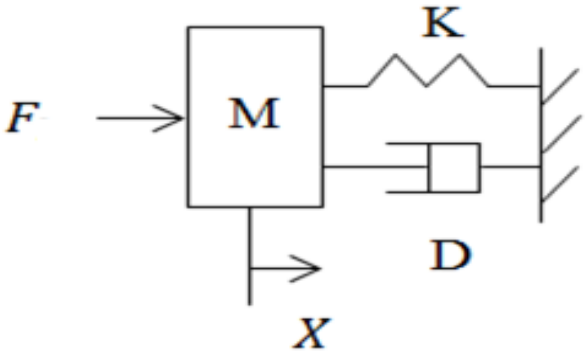

Fig. 4.3: Mass-damper-spring model.

The mathematical formula of the compliance model can be derived from Newton's second laws, as shown in below:

$$\sum F = M\ddot{x} \tag{4.1}$$

$$F = M\ddot{x}_k + D\dot{x}_k + Kx_k \tag{4.2}$$

where M, D and K are the desired mass coefficient, desired damper coefficient, desired spring coefficient, respectively. Then k represents each sampling time point and F represents the actual sampling time point of contact force on the robot end-effector. Then we have,

$$\dot{x}_k = \frac{x_k - x_{k-1}}{\Delta t} \tag{4.3}$$

$$\ddot{x}_k = \frac{\dot{x}_k - \dot{x}_{k-1}}{\Delta t} = \frac{x_k - 2x_{k-1} + 2x_{k-2}}{\Delta t^2} \tag{4.4}$$

where x, $\dot{x}$, $\ddot{x}$ and Δt are the robot end-effector position, velocity, acceleration and

sampling interval respectively.

Substituting the equation (4.3) and (4.4) into (4.2), we obtain

$$x_k = x_k^{cmd} = \frac{F\cdot\Delta t^2+(2M+\Delta t\cdot D)\cdot x_{k-1}-M\cdot x_{k-2}}{\Delta t^2\cdot K+M-\Delta t\cdot D} \quad (4.5)$$

4.3 Simulation of Compliance Model

As previous mentioned, the compliance model consists of three paramters: mass coefficient (M), damper coefficient (D) and spring coefficient (K), these parameters would affect the compliance level of robot hand. In this section, we will discuss the influence of compliance level by tuning these parameters. We changed the parameter of M, D and K respectively and simulated the compliance model by MATLAB. In Fig. 4.4, we set parameters of F, D and K are 5N, 5 Ns/m and 100 N/m respectively.

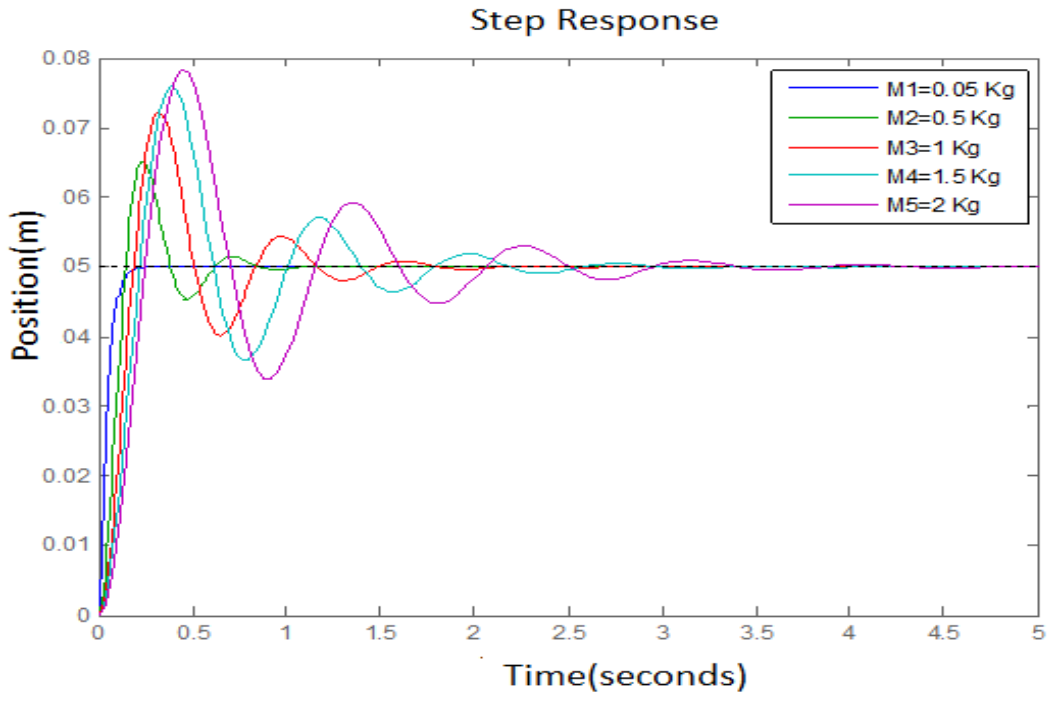

Fig. 4.4: Step respond of various M correspond to position.

The parameters of M are 0.05 Kg, 0.5 Kg, 1 Kg, 1.5 Kg and 2 Kg. Applied the same input of force, when the parameter of M became smaller, it means that the load is small, the responding time of system is fast and overshoot decreased. Conversely, the time respond of system is slow and overshoot increase and when the parameter of M is getting bigger. In Fig. 4.5, we set parameters of F, M, and K are 5N, 0.5 Kg and 100 N/m respectively. The parameters of D are 1 Ns/m, 5 Ns/m, 10 Ns/m, 15 Ns/m and 20 Ns/m. Applied the same input of force, when the parameter of D becomes smaller, it means the viscous force is small, the settling time of system is long and overshoot increased. Conversely, the settling time of system is short and overshoot decrease when the parameter of D is getting bigger.

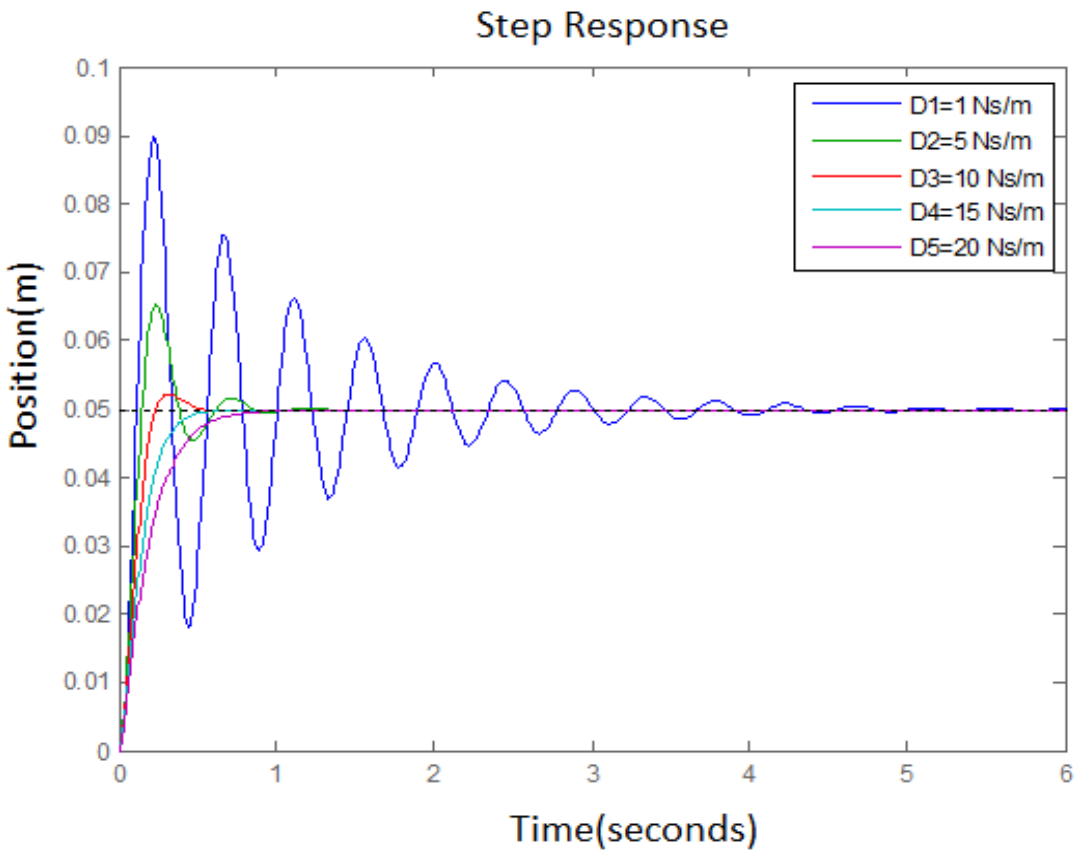

Fig. 4.5: Step respond of various D correspond to position.

In Fig. 4.6, we set parameters of F, M and D are 5N, 0.5 Kg and 5 Ns/m respectively. The parameters of K are 10 N/m, 20 N/m, 50 N/m, 100 N/m and 200 N/m. Applied the same input of force, when the parameter of K becomes smaller, it means the stiffness is low, the robot hand can easily move by the external force. Thus, there is no oscillation occurs error and the steady state error of system increase. Conversely, when the parameter of K is getting bigger the oscillation occurs in trasient response and the steady state error of system decrease.

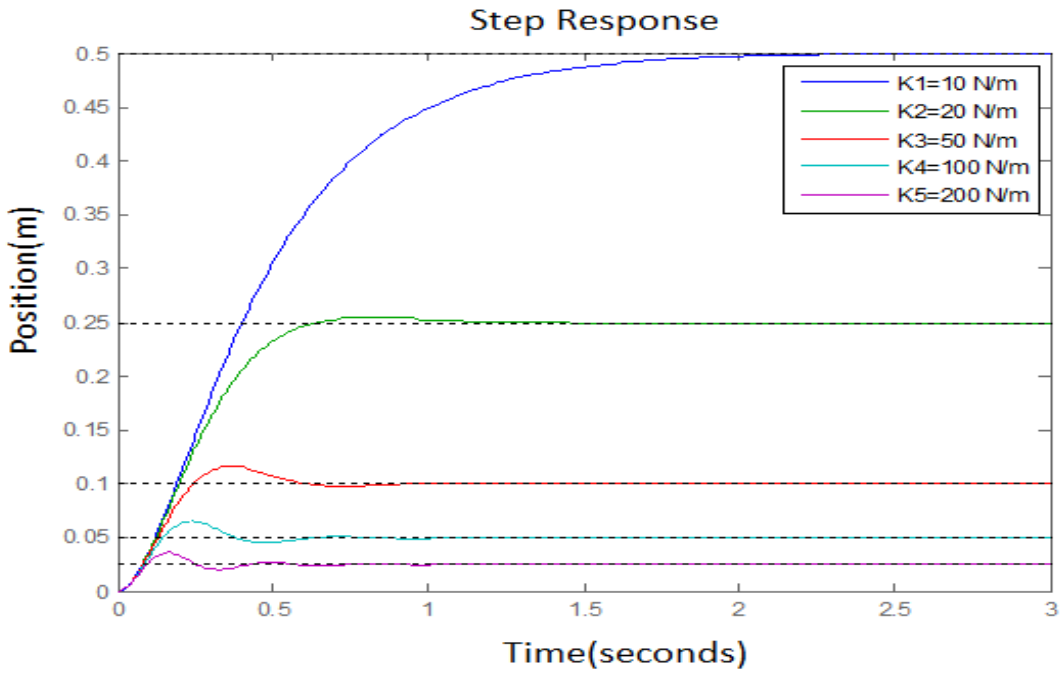

Fig. 4.6: Step respond of various K correspond to position.

V. Experimental Results

In this chapter, we will validate the mechanism design for finger-movement control. After that, we will present the experimental results of safety task-orientation training for grasping, which is divided into user compliance control and grasping compliance control. The experiment of user compliance control aims to check if the design can allow the patient to control the movement of robotic fingers freely. In addition, the experiment of grasping compliance control demonstrates that a user grasping different weights of balls can be assisted by the hand exoskeleton effectively. At last, we will investigate the response survey from the users after using this robotic device.

5.1 Validation of Mechanism Design for Movement Control

In this experiment, we will test the movement of hand exoskeleton with pure position control to validate the function of hand exoskeleton. The test of fingers motion is shown in Fig. 5.1, the hand exoskeleton was placed on the table without user wearing and set up to a stretched posture (joint position equal to zero) in the beginning. The robotic index finger movement is shown in Fig. 5.1 (a) ~ (b). The robotic thumb movement is shown in Fig. 5.1 (c) ~ (d). In Fig. 5.2, the recorded positions of linear motors show that the robotic fingers are driven by the linear motors successfully with pure position control experiment.

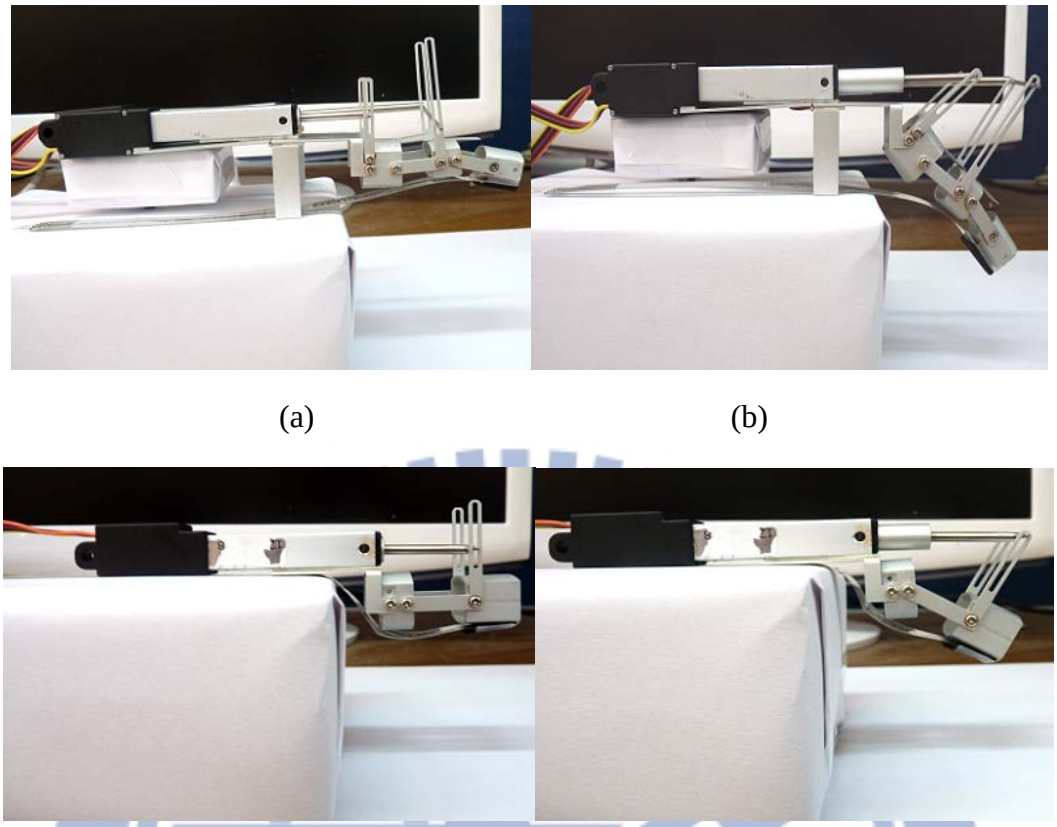

(a) (b)

(c) (d)

Fig. 5.1: Test of fingers motion (a) Initial posture of robotic index finger (b) End posture of robotic index finger (c) Initial posture of robotic thumb (d) End posture of robotic thumb.

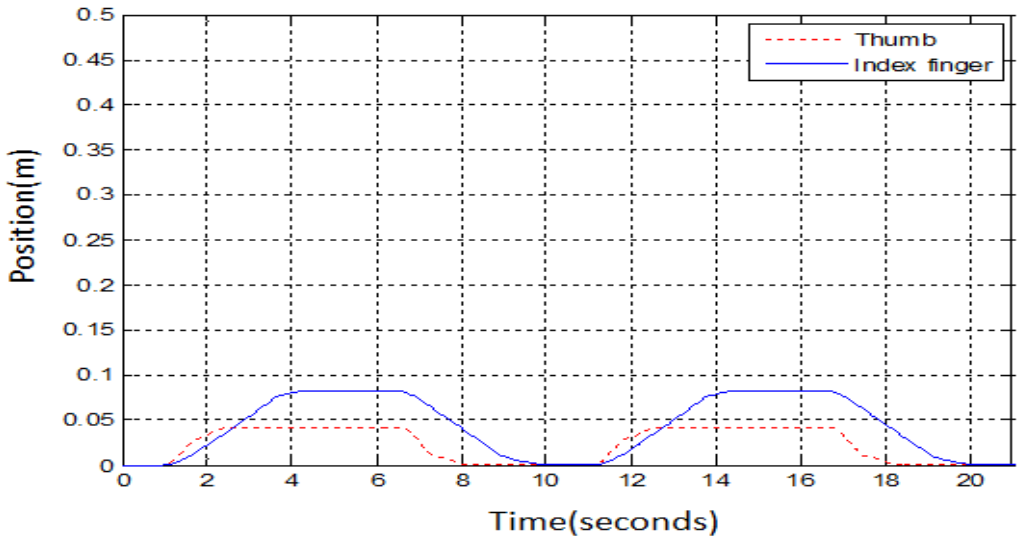

Fig. 5.2: Experiment results of pure position control.

5.2 Experiment of Safety Task-oriented Training

This experiment simulated that the patients are required to try their best effort to achieve the grasping task. Fig. 5.3 shows the picture of task-oriented training in grasping. The scenario of grasping the task-orientation training in this experiment is explained as follows:

1. The patient sits in front of the table and tries to grasp a ball at the initial point.

2. Lift the ball and move to the end point, the distance between the initial point and the end point is 15 centimeter (cm).

3. Release the ball on the table when reaching the end point. After completion, repeat the procedure by lifting the ball from the end point and place it back to the initial point again.

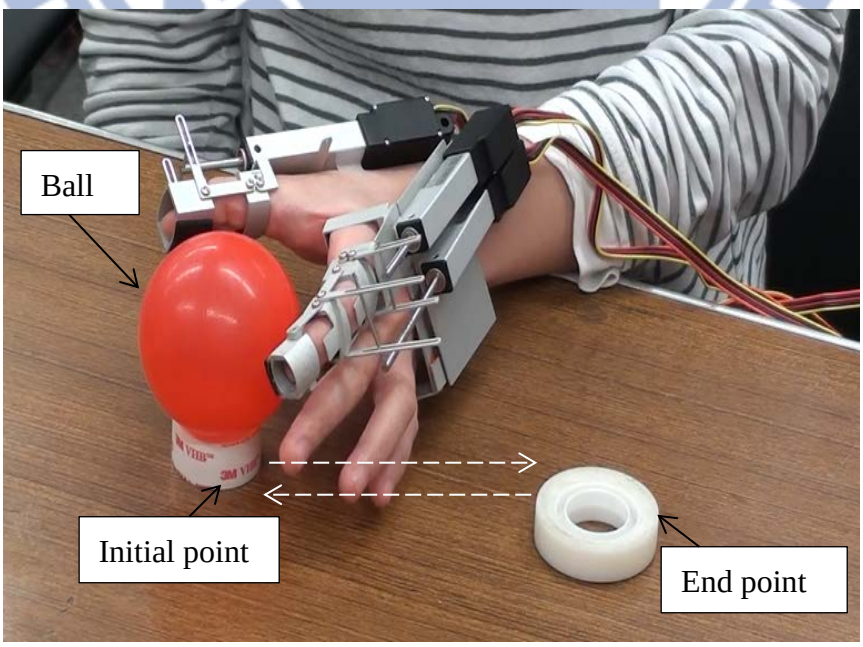

Fig. 5.3: Illustration of task-oriented training for a grasping task.

The experiment of safety task-oriented training is composed of two compliant control modes: user compliance control and grasping compliance control. Fig. 5.4 shows the finite state machine of task-oriented training in grasping task. The behavior of state machine will be described as follow:

1. The robotic fingers standby with pure position control (with initial joint angle equal to zero) if finger pressing force $\leq$ threshold value.

2. The system will execute the user compliance control mode if the finger pressing force exceeds a threshold value. The motion of robotic fingers will follow the direction of the user's force to move to reach the object.

3. The system will switch to grasping compliance control mode if the object contact force exceeds a threshold value. The robotic fingers assist the user to grasp the object. Otherwise, the system will continue to execute the user compliance control until the object force exceeds the threshold value, if the finger pressing force exceeds a threshold value. In this state, the user is supposed to lift and move the object to the target point.

4. The robotic fingers release the object at the target point if the finger pressing force decreases (with no intention to hold the object any more).

5. After completion, the system will return to the standby mode to check the user's intention force again.

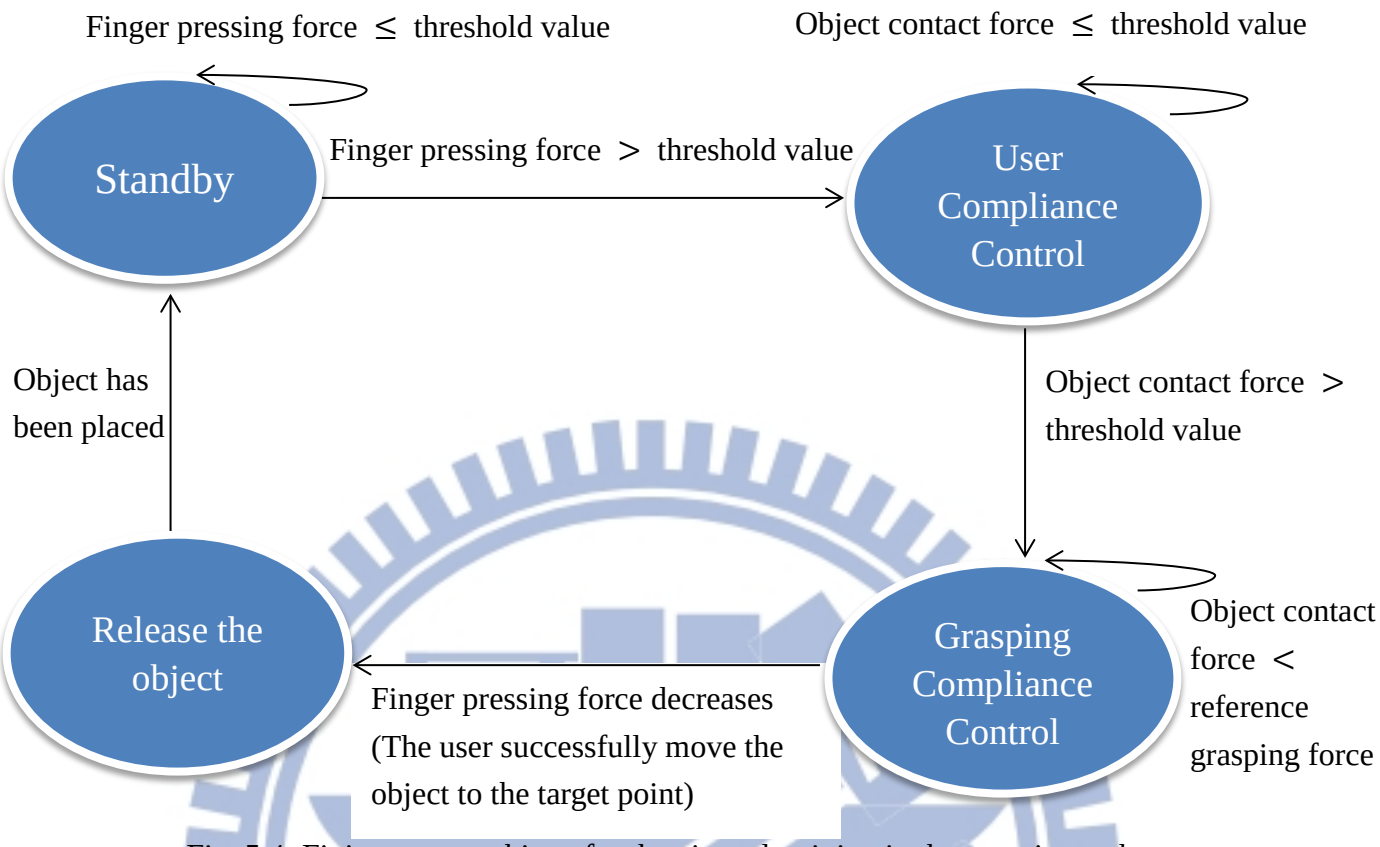

Fig. 5.4: Finite state machine of task-oriented training in the grasping task.

5.2.1 Experiment of User Compliance Control

The purpose of this experiment is to demonstrate the compliance control force to perform the compliance motion of robotic finger by exerting a human force. In the experiment, the motion of robotic finger would follow the user's active force and convert it to the finger's motion. A force sensor was mounted inside the end-effector of an index robotic finger that can only be detected by the vertical direction when contact by human finger. The parameter of compliance model M, D, K is set as 0.04 Kg, 0.6 Ns/m and 0.8 N/m respectively. The demonstration of this experiment is shown in Fig. 5.5. The user exerts a force to control the movement of the robotic finger. The robotic fingers start flexion in Fig. 5.5 (a) ~ (c) and the robotic fingers extended as shown in Fig. 5.5 (d) ~ (e). The movement of flexion and extension will repeat again in Fig. 5.5 (f) ~ (i).

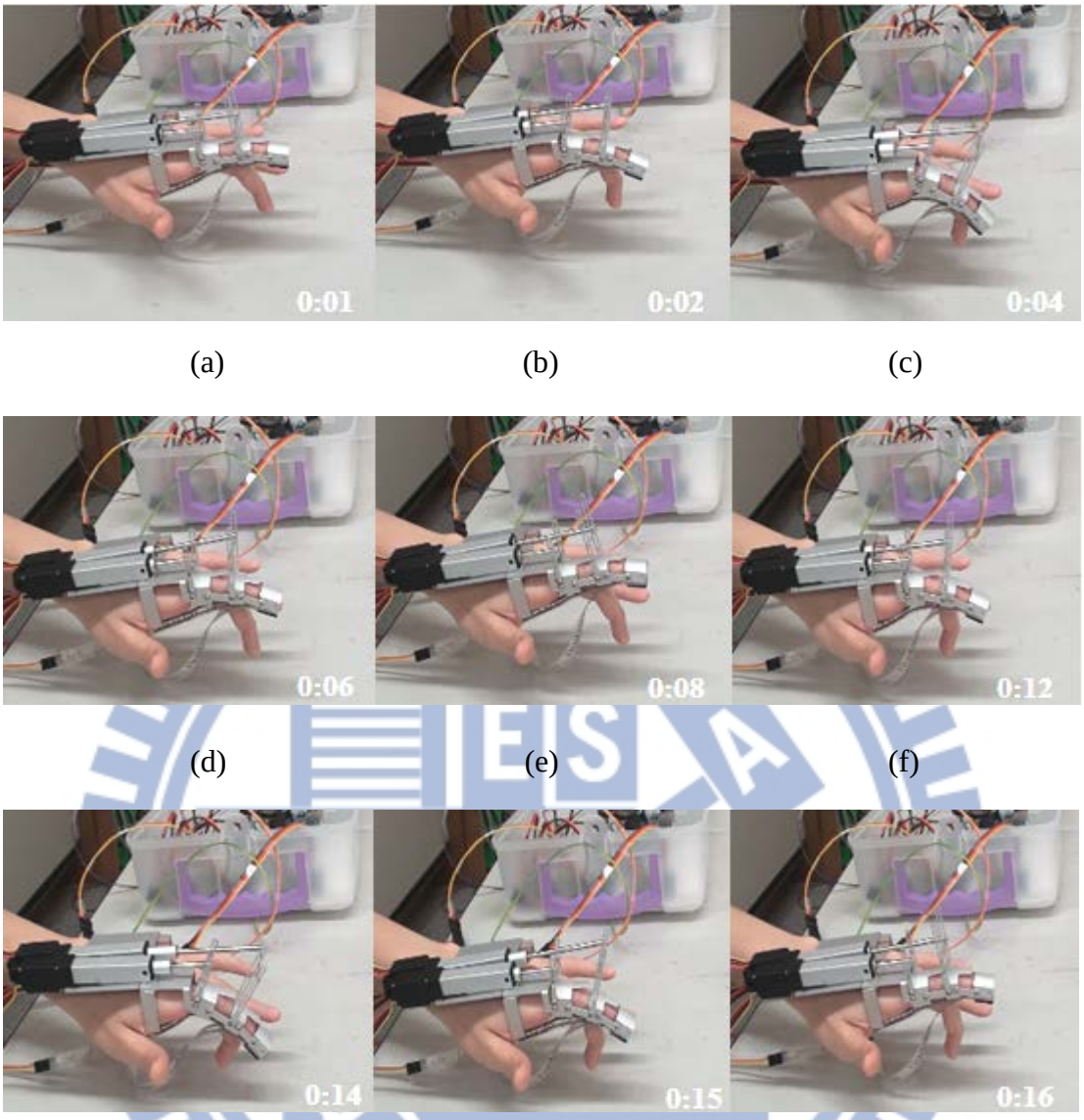

Fig. 5.5: Demonstration of user compliance control.

Fig. 5.6 is shows the experiment results of user compliance control. In Fig. 5.6 (a), the user exerts a force to exoskeleton at 2 seconds and releases the finger at 5 seconds, after a few seconds the user exert a force again at 12 seconds and releases the finger at 15 seconds. Fig. 5.6 (b) is shows the position response from the user's active force, green solid line is the actual position of the end effector of robotic finger. In Fig. 5.6, it is shown that the motions of robotic fingers are controlled by the patient's intention.

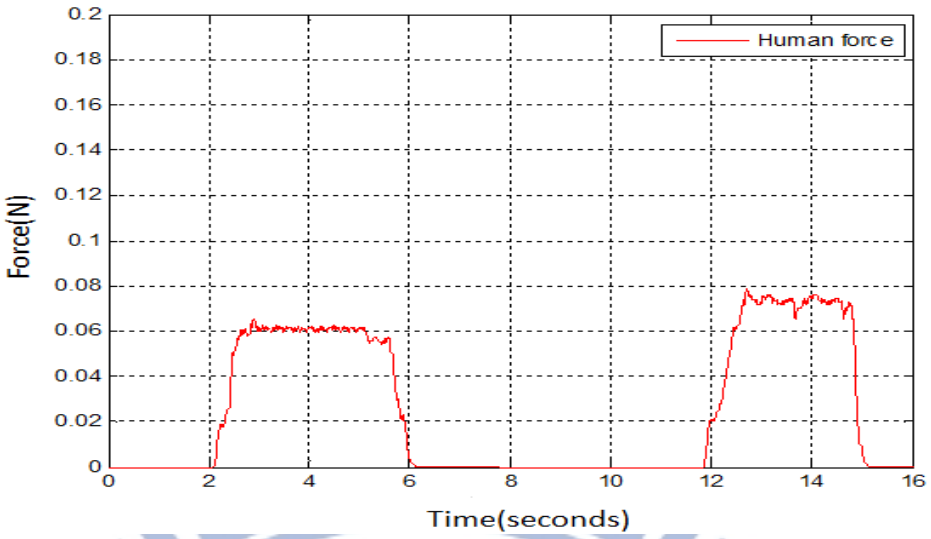

(a)

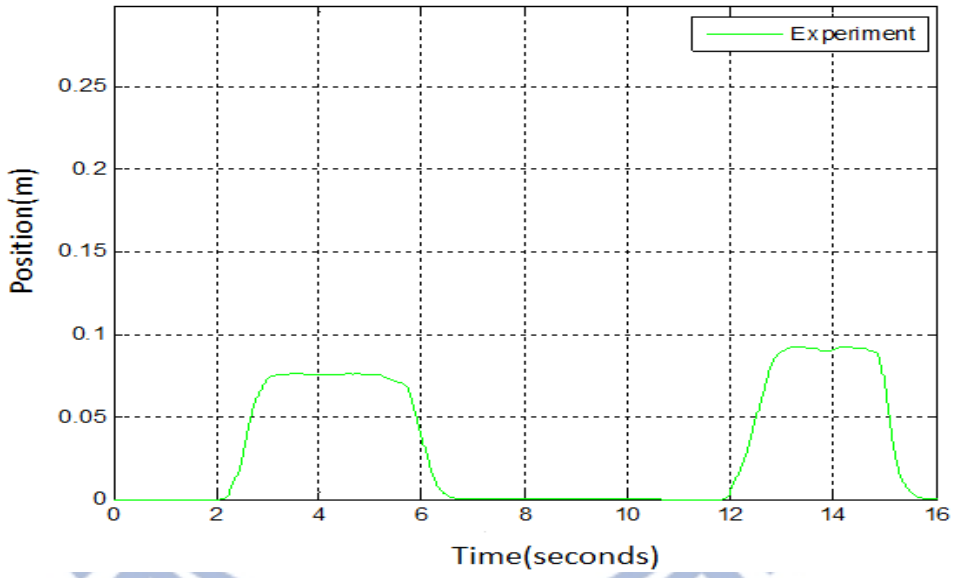

(b)

Fig. 5.6: Experiment results of user compliance control
(a) Force response (b) Position response.

5.2.2 Experiment of Grasping Compliance Control

The purpose of this experiment is to target and change the compliance control force to perform compliance motion of robotic hand that can assists the patient to grasp different weights of balls. Two different balls that weights 20g and 80g were tested in this experiment. The compliance force will be executed to assist the desired

grasping force depends on the weight of ball when the robotic hand contact with the ball. Besides, the reference force in both experiments are setting based on the investigated object. Two sensors were installed at the end-effector of each robotic finger for measuring the human contact force and robotic contact force. The compliance controller parameter for a 20g of ball and compliance controller parameter for an 80g is shown in Table 5.1 and Table 5.2 respectively. The demonstration of grasping compliance control for a 20g of ball and grasping compliance control for an 80g is shown in Fig. 5.7 and Fig. 5.8 respectively.

Table 5.1: Parameter of compliance controller for a 20g ball.

Parameter setting	Desired Force (N)	M (Kg)	D (Ns/m)	K (N/m)
Index finger	0.12	0.04	10	40
Thumb	0.12	0.02	10	40

Table 5.2: Parameter of compliance controller for an 80g ball.

Parameter setting	Desired Force (N)	M (Kg)	D (Ns/m)	K (N/m)
Index finger	0.42	0.04	10	42
Thumb	0.42	0.02	10	42

(a) (b) (c)

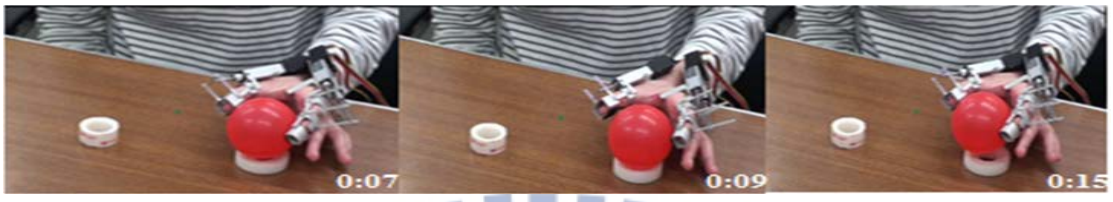

(d) (e) (f)

(g) (h) (i)

Fig. 5.7: Demonstration of grasping compliance control for a 20g ball.

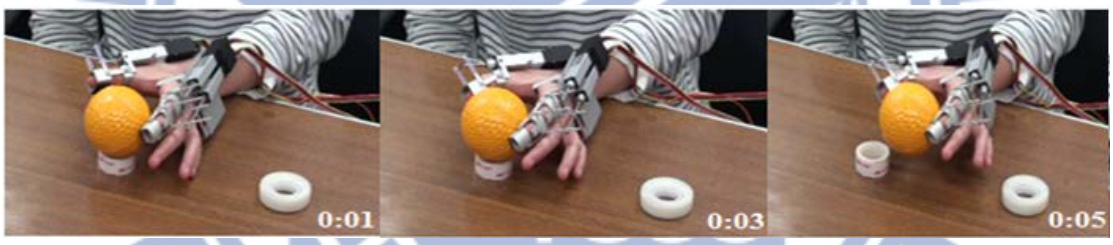

(a) (b) (c)

(d) (e) (f)

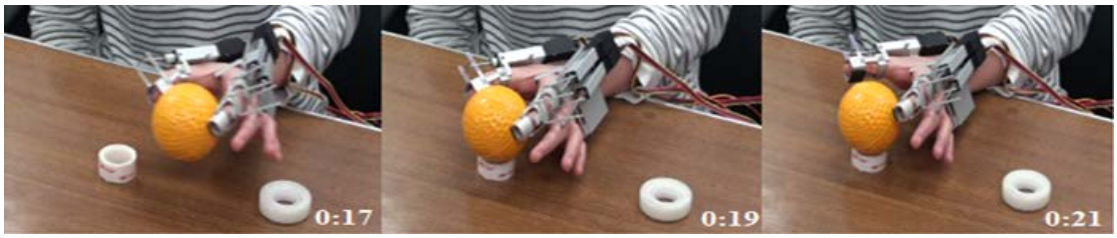

(g) (h) (i)

Fig. 5.8: Demonstration of grasping compliance control for an 80g ball.

The robotic fingers start grasping ball and move to the end point in Fig. 5.7 (a) ~ (d) and Fig. 5.8 (a) ~ (d) respectively. The robotic fingers release the ball in Fig. 5.7 (e) and Fig. 5.8 (e) respectively. After that, the robotic fingers will grasp the ball again from end point to initial point in Fig. 5.7 (f) ~ (i) and Fig. 5.8 (f) ~ (i) respectively. The experiment results of grasping compliance control for a 20g ball is shown in Fig. 5.9. In Fig. 5.9 (a), red dotted line is the reference grasping force we give. The blue

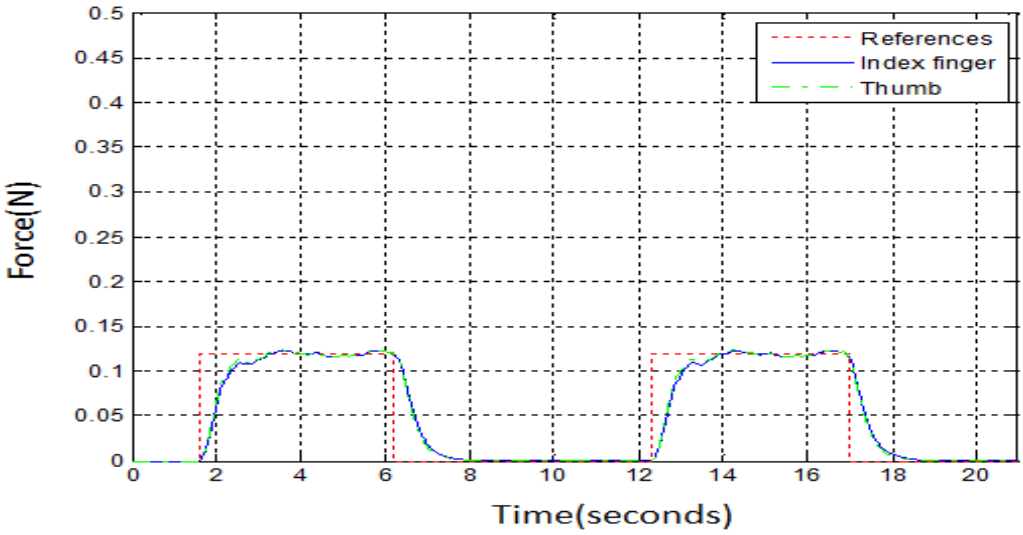

(a)

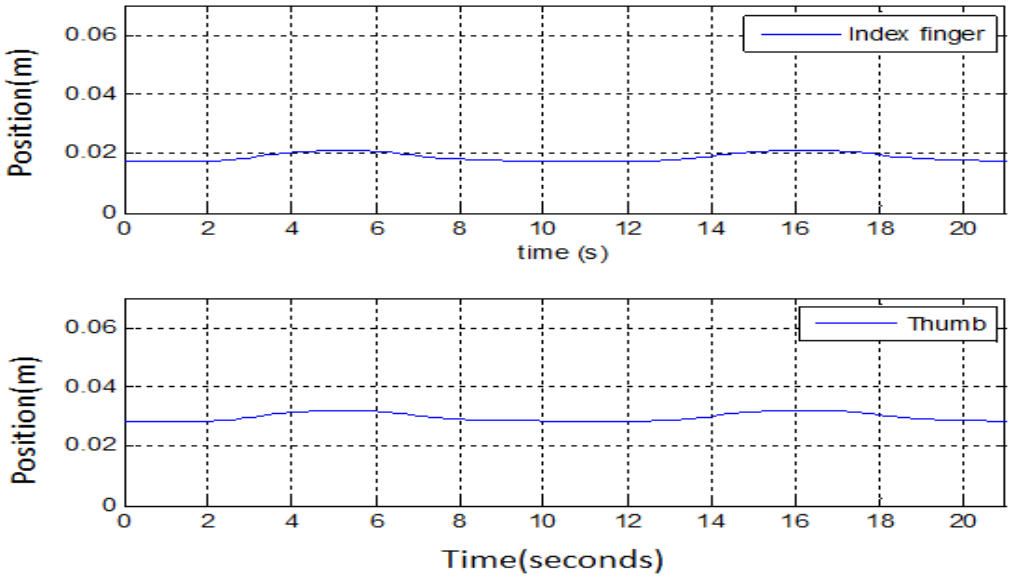

(b)

Fig. 5.9: Experiment results of grasping compliance control for a 20g ball (a) Force response (b) Position response.

solid line and green dotted line is the actual contact force from robotic index finger and robotic thumb respectively. Fig. 5.9 (b) is shown the position response of grasping compliance control for a 20g ball, blue solid line is the actual position of the end effector of robotic fingers.

The experiment results of grasping compliance control for an 80g ball is shown in Fig. 5.10. In Fig. 5.10 (a), red dotted line is the reference grasping force we give. The blue solid line and green dotted line is the actual contact force from robotic index finger and robotic thumb respectively. Fig. 5.10 (b) is shown the position response of grasping compliance control for an 80g ball, blue solid line is the actual position of the end effector of robotic fingers. From these result, it is clearly shown that the robotic fingers capable to grasp different weights of balls through the compliance controller.

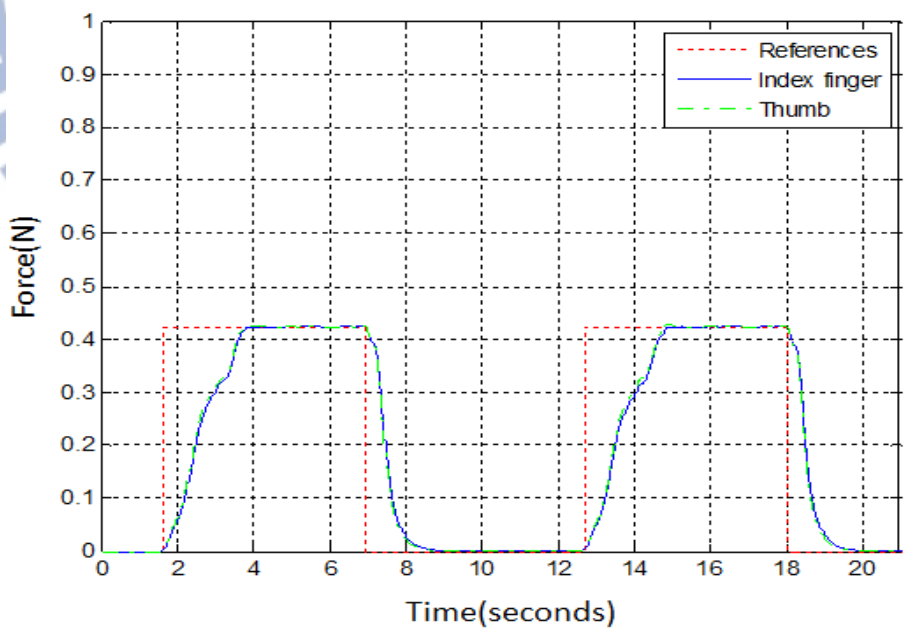

(a)

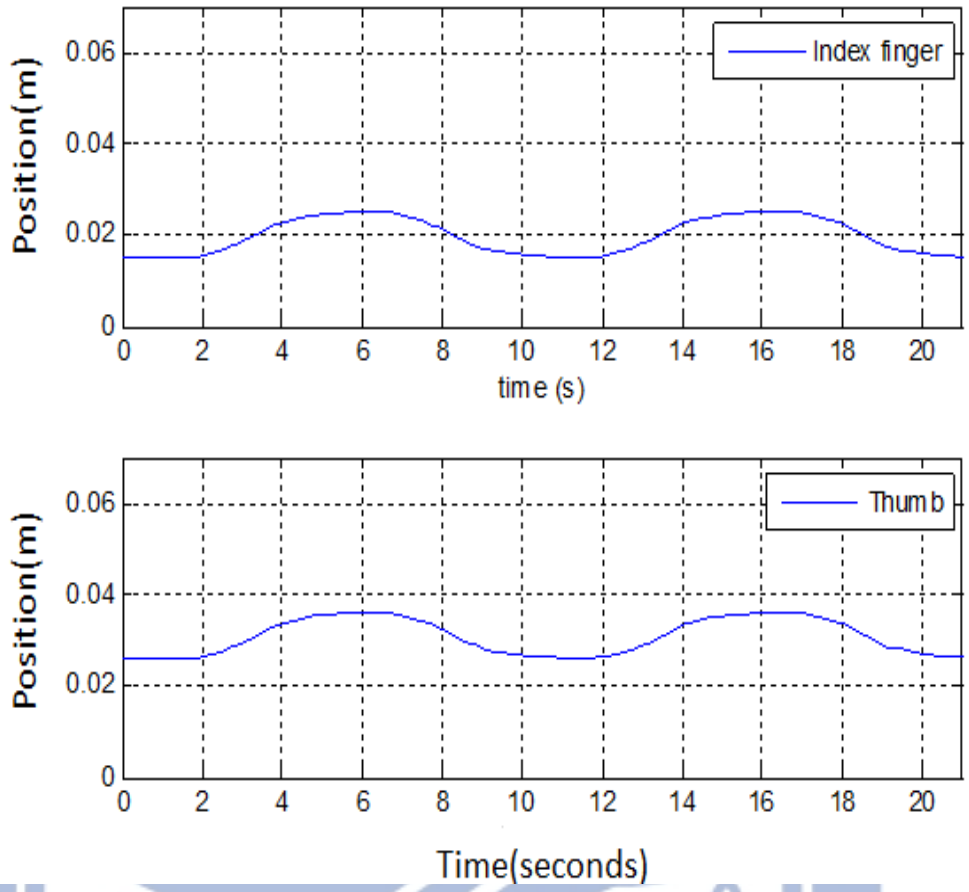

(b)

Fig. 5.10: Experiment results of grasping compliance control for an 80g ball (a) Force response (b) Position response.

5.2.3 Discussion about the Experiments

In the section one of this chapter is the experiment of user compliance control, the user can easily control the movement of robotic finger with their active force. When the user exerted an active force, the compliance model will generate a desired position in Fig. 5.6 (b). From this experiment, we can clearly observe that the motion of robotic finger is compliance with the user's active force for achieving comfortable wearing.

In the section two of this chapter is the experiment of grasping compliance control for grasping different weights of balls. In Fig. 5.9 and Fig. 5.10, we can observe that the positions are proportional to the applied force. From these results, the

force and position output are well agreed with the references values in experiment of grasping compliance control for grasping different weights of balls. The grasping compliance motion was truly achieved by compliance control based on the investigated object. Moreover, the robotic fingers are capable to assist the patient to grasp the different weights of balls and provide a safety environment for the task training.

5.3 User Survey for Performance Evaluation

The purpose for this section is to examine the performance result of our design. We have selected five healthy persons to use our device to complete the task-oriented training for grasping task. After completion, we asked some questions in order to investigate the feedback response of our design. Table 5.3 is the profile of participants and Table 5.4 is our survey questions for the design.

Table 5.3: Profile of participants.

No.	Age	Gender	Height (cm)
1	20	Female	158
2	22	Male	166
3	22	Female	163
4	38	Female	160
5	41	Female	162

Table 5.4: Survey questions for the design.

	Extremely satisfied	Very satisfied	Neutral	Not very satisfied
Do you feel comfortable with our device?				
Do you feel safe using our device?				
Are you able to control the hand exoskeleton easily?				
Do you feel satisfied with the assistive performance of this device?				
Do you feel burden with the weight of hand exoskeleton?				

Fig. 5.11 shows the results of this survey, the result of comfortable rate is 83.5%, safety rate is 85.4%, performance of intention control is 86% and performance of assistive is 87%. On the basic of these findings, it seems that the users who had used our device are satisfied with our design. However, the comfortable rate is the lowest, so that we could improve the comfortable of our device.

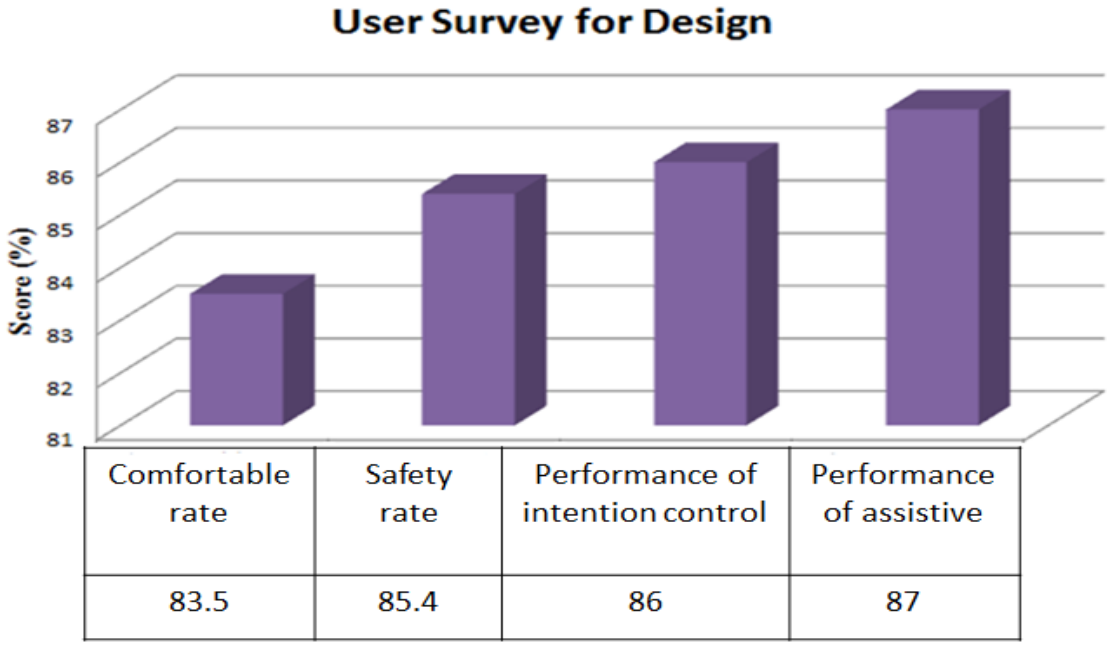

Fig. 5.11: The survey results.

VI. Conclusion and Future Work

6.1 Conclusion

This wearable rehabilitation robotic fingers design is to assist the stroke patient to attain the grasping task for helping them to regain motor skills and functions. The main purpose for this safety control strategy is to allow the user participate in control of exoskeleton device according to their intention active force and provide an assistive grasping force to ensure the user grasping the object without any damaged during training. In this thesis, we accomplished the design of a two-finger system including the mechanical design, hardware system architecture and compliance system architecture. The mechanical design functions for these robotic fingers are according to human hand anatomy which provides the flexion/extension movement. We analyze the kinematics of two robotic fingers in order to position the robotic finger to execute the grasping task. In addition, a compliance control for robotic fingers was implemented considering the human-robot interaction (user compliance control) and robot-environment interaction (grasping compliance control). From the experiment of user compliance control, the compliance control parameter was considered based on impedance characteristics of human finger. Furthermore, the compliance controls of grasping based on different weights of objects have been successfully demonstrated. From the above results, it is proven that the wearable rehabilitation robotic finger is capable to assist the stroke patient to grasp the different weights of objects safely.

6.2 Future Work

Currently, we have only designed the robotic thumb and index finger for the stroke patients. In the future, we are going to invent further for the five fingers to improve the hand exoskeleton functioning together. The considerations of gravity

compensation and disturbance resistance capabilities are important to guarantee a firm grasping. It will also be interesting to conduct satisfaction survey to verify the assistive performance of exoskeleton device with different control algorithm, for example compare the compliance control and pure position control which applied in exoskeleton device. Furthermore, more practical experiments on patients and evaluation of hand rehabilitation will be studied in future.

References

[1] 台大醫院衛教資料:“台灣腦血管疾病的現況”
http://www.ntuh.gov.tw/neur/衛教資料/DocLib2/中風的預防/臺灣腦血管疾病的現況.aspx

[2] America National Stroke Association.
http://www.stroke.org/site/PageNavigator/HOME

[3] D. W. Duncan, R.K. Bode, S. Min Lai and S. Perera, “Rasch Analysis of a New StrokeSpecific Outcome Scale: the Stroke Impact Scale,” *Archives of Physical Medicine Rehabilitation*, Vol. 84, pp. 950-63, 2003.

[4] V. W. Mark and E. Taub, “Constraint-induced Movement Therapy for Chronic Stroke Hemiparesis and Other Disabilities,” *Restorative Neurology and Neuroscience*, Vol. 22, No. 3-5, pp.317-336, 2004.

[5] R. Tubiana, J. M. Thomine and E. Mackin, *Examination of the Hand and Wrist, 2nd ed.*, Taylor & Francis, 1998.

[6] Donald A. Neumann, *Kinesiology of the Musculoskeletal System: Foundations for Rehabilitation, 2nd ed.*, Mosby Elsevier, 2010.

[7] DR.Tummy.com.
http://drtummy.com/index.php?option=com_content&view=article&catid=84:headers&id=321:bones-of-the-hand&Itemid=58

[8] Y. Wu and T. S. Huang, “Human Hand Modeling, Analysis and Animation in the Context of HCI,” in *Proc. of International Conference on Image Processing*, Kobe, Japan, 1999, pp. 6-10.

[9] Whitney Lowe, *Orthopedic Assessment in Massage Therapy*, Daviau-Scott, 2006.

[10] J. Lee and T. Kunii, “Model-based Analysis of Hand Posture,” *IEEE Computer Graphics and Applications*, vol.15, pp. 77-86, 1995.

[11] National Institute of Neurological Disorders and Stroke: Post-Stroke Rehabilitation Fact Sheet. http://www.ninds.nih.gov/disorders/stroke/poststrokerehab.htm

[12] M. Rensink, M. Schuurmans, E. Lindeman and T. Hafsteinsdóttir, "Task-oriented Training in Rehabilitation After Stroke: Systematic Review," *Journal of Advanced Nursing*, Doi: 10.1111/j.1365-2648.2008.0429.x, 2009.

[13] A. A. A. Timmermans, H. A. M. Seelen, R. P. J. Geers, P. K. Saini, S. Winter, J. te Vrugt and H. Kingma, "Sensor-based Arm Skill Training in Chronic Stroke Patients: Result on Treatment Outcome, Patient Motivation, and System Usability," *IEEE Transactions on Neural System and Rehabilitation*, Vol.18, pp.284-292, 2010.

[14] Joel Stein, Richard L. Harvey, Richard F. Macko, Carolee J. Winstein and Richard D. Zorowitz, *Stroke Recovery and Rehabilitation*, Demos Medical, 2008.

[15] N. Maclean, P. Pound, C. Wolfe, A. Rudd, "Qualitative Analysis of Stroke Patients' Motivation for Rehabilitation," *British Medical Journal*, 321:1051-1054, 2000.

[16] J. J. Park, Y. J. Lee, J. B. Song and H. S. Kim, "Safe Joint Mechanism Based on Nonlinear Stiffness for Safe Human-Robot Collision," in *Proc. of IEEE International Conference on Robotics and Automation*, Pasadena, CA, 2008, pp. 2177-2182.

[17] J. J. Park, H. S. Kim and J. B. Song, "Safe Robot Arm with Safe Joint Mechanism using Nonlinear Spring System for Collision Safety," in *Proc. of IEEE International Conference on Robotics and Automation*, Kobe, Japan, 2009, pp. 3371-3376.

[18] J. J. Park and J. B. Song, "Safe Joint Mechanism using Inclined Link with Springs for Collision Safety and Positioning Accuracy of a Robot Arm," in *Proc. of IEEE International Conference on Robotics and Automation*, Anchorage, Alaska, U.S., 2010, pp. 813-818.

[19] N. Hogan, "Impedance Control: an Approach to Manipulation. Part I: Theory,

Part II: Implementation, Part III: Application," *Transaction of ASME, Journal of Dynamic Systems, Measurement, and Control*, vol.107, pp. 1-23, 1985.

[20] H. Kazerooni, "Robust Compliant Motion：Impedance Control," in *Proc. of IEEE Conference on Robotics and Automation*, Albuquerque, New Mexico, U.S., 1986, pp.185-188.

[21] R. J. Anderson and M. W. Spong, "Hybrid Impedance Control of Robotics Manipulators," *IEEE Transactions on Robotics and Automation*, Vol.4, No.5, pp.549-556, 1988.

[22] G. J. Liu and A. A. Goldenberg, "Robust Hybrid Impedance Control of Robot Manipulators," in *Proc. of IEEE Conference on Robotics and Automation*, CA, USA, 1991, pp.287-292.

[23] Y. Yang, L. Wang, J. Tong and L. Zhang, "Arm Rehabilitation Robot Impedance Control and Experimentation," in *Proc. of IEEE Conference on Robotics and Biomimetics*, Kunming, China, 2006, pp. 914-918.

[24] J. Jalani, G. Herrmann and C. Melhuish, "Robust Active Compliance Control for Practical Grasping of a Cylindrical Object via a Multifingered Robot Hand," in *Proc. of IEEE 5th International Conference on Robotics, Automation and Mechatronics (RAM)*, Qingdao, China, 2011, pp. 316-321.

[25] R. Paul and B. Shimano, "Compliance and Control," in *Proc. of Joint Automation Control Conference*, New York, 1976, pp.694-699.

[26] J. J. Craig and M. H. Raibert, "Hybrid Position/Force Control of Manipulators," *Journal of Dynamic Systems, Measurement and Control*, Vol.102, pp. 126-133, 1981.

[27] M. T. Mason, "Compliance and Force Control for Computer Controlled Manipulators," *IEEE Transactions on Systems, Man, and Cybernetics*, Vol.11, No. 6, pp. 418-432, 1981.

[28] M. H. Raibert and J. J. Craig, "Hybrid Position/Force Control of Manipulators," *Journal of Dynamic Systems, Measurement and Control, Transactions of the ASME*, Vol.103, pp. 275-282, 1981.

[29] S.Parasuraman, Arif Wicaksono Oyong and Velappa Ganapathy, “Development of Robot Assisted Stroke Rehabilitation System of Human Upper Limb,” in *Proc. of 5th Annual IEEE Conference on Automation Science and Engineering*, Bangalore, India, 2009, pp. 256-261.

[30] Yupeng Ren, Hyung-Soon Park and Li-Qun Zhang, “Developing a Whole-Arm Exoskeleton Robot with Hand Opening and Closing Mechanism for Upper Limb Stroke Rehabilitation,” in *Proc. of 11th International Conference on Rehabilitation Robotics*, Kyoto, Japan, 2009, pp. 761-765.

[31] Y. Hasegawa, Y. Mikami, K. Watanabe and Y. Sankai, “Five-Fingered Assistive Hand with Mechanical Compliance of Human,” in *Proc. of IEEE International Conference on Robotics and Automation*, Pasedena, CA, USA, 2008, pp. 718-724.

[32] Kexin Xing, Qi Xu and Yongji Wang, “Design of Wearable Rehabilitation Robotic Hand Actuated by Pneumatic Artificial Muscles, ” in *Proc. of 7th Asian Control Conference*, Hong Kong, China, 2009, pp. 740-744.

[33] H. Yamaura, K. Matsushita, R. Kato and H. Yokoi, “Development of Hand Rehabilitation System Using Wire-Driven Link Mechanism for Paralysis Patients, ” in *Proc. of IEEE International Conference on Robotics and Biomimetics*, Guilin, China, 2009, pp. 209-214.

[34] Yili Fu, Qinchao Zhang, Fuhai Zhang and Zengkang Gan, “Design and Development of a Hand Rehabilitation Robot for Patient-cooperative Therapy Following Stroke, ” in *Proc. of IEEE International Conference on Mechatronics and Automation*, Beijing, China, 2011, pp. 112-117.

[35] N. S. K. Ho, K. Y. Tong, X. L. Hu, K. L. Fung, X. J. Wei, W. Rong and E. A. Susanto, “An EMG-driven Exoskeleton Hand Robotic Training Device on Chronic Stroke Subjects-Task Training System for Stroke Rehabilitation, ” in *Proc. of IEEE International Conference on Rehabilitation Robotics Rehab Week Zurich*, ETH Zurich Science City, Switzerland, 2011, pp. 125-129.

[36] J. H. Bae, Y. M. Kin and I. Moon, “Wearable Hand Rehabilitation Robot Capable of Hand Function Assistance in Stroke Survivors,” in *Proc. of IEEE 4th RAS/EMBS International Conference on Biomedical Robotics and*

Biomechatronics, Roma, Italy, 2012, pp. 1482-1487.

[37] Arduino Official Website.
http://arduino.cc/en/Main/ArduinoBoardMega2560

[38] Firgelli Technology Inc. Miniature Linear Motion Series.
http://www.firgelli.com/Uploads/L12_datasheet.pdf

[39] Firgelli Technology Inc. Firgelli Linear Actuator Control Board.
http://www.firgelli.com/Uploads/LAC_Datasheet.pdf

[40] Tekscan Inc.
http://www.tekscan.com/pdf/A201-force-sensor.pdf

[41] John J. Craig, *Introduction to Robotics: Mechanics and Control, 3rd ed.*, Pearson Education, 2005.